Modelling Simul. Mater. Sci. Eng. 2 (1994) 167–184. Printed in the UK

A stochastic model for continuum elasto-plastic behavior: I. Numerical approach and strain localization

V V Bulatov† and A S Argon
Massachusetts Institute of Technology, Cambridge, MA 02139, USA

Received 26 January 1993, accepted for publication 3 August 1993

Abstract. A 2D model, in which plastic flow is treated as a stochastic sequence of local inelastic transformations, is proposed. In this model internal elastic stresses, resulting from such inelastic transformations, are explicitly accounted for, and an effective computer code for numerical simulation of plastic flow at arbitrary temperature and loading conditions is developed. The transition from diffuse high-temperature flow to well localized low-temperature flow is a natural result of the model. Various kinetic and structural aspects of plasticity in the model 2D solid at different temperatures are discussed. The model that is developed is primarily initiation controlled, and represents well the properties of amorphous media. It is to be distinguished from mobility-controlled plasticity involving dislocation glide. In its manifestations, however, the distinction becomes blurred.

1. Introduction

It is a commonly accepted point of view now that macroscopically observable plastic flow in amorphous solids is a net result of individual structural alterations occurring on the scale of a few atoms or molecular groups.

Different plastic solids show, in general, some differences in macroscopic behavior, which indicates that the very intimate mechanisms of plasticity in them are often *structurally specific*. At the same time, various qualitative features of plasticity are remarkably similar for solids of different chemical composition and packing structure. A very effective way of studying structurally specific microscopic mechanisms of inelastic processes in solids is to use various techniques of atomic level modeling. Several models of this kind have been studied in the past—with some of them being quite realistic in terms of the chemical structures they were supposed to represent [1–5].

While atomic-level simulations have provided many thought-provoking results, length scales and time intervals available for modeling with such a degree of detail are still very much shorter than those corresponding to the macroscopic processes. At the same time, as mentioned above, qualitative similarity of plastic flow in different solids implies that a reasonable common description of these processes might be given within less detailed considerations.

In the present paper we propose a model, in which plastic flow is treated as a stochastic sequence of *local inelastic transformations* (LITs), considered here and afterwards as the smallest flow elements (representative volume elements) of the plastic solid. This approach enables us to perform numerical simulations of plastic flow at much larger length scales

† On leave from the Institute of Chemical Physics, Russian Academy of Sciences, Moscow, Russia.

0965-0393/94/020167+18$19.50

and for much longer time intervals†. What is worth noting is that all parameters of the model (geometry and energetics of individual LITs) may be obtained from more detailed atomic-level simulations.

In what follows we make an attempt to develop an idealized model of a solid for the purpose of examining the principal capability of our approach to account for those features of plastic flow that are qualitatively the same for all plastic solids, regardless of their chemical composition or structural make-up. Therefore, we try to keep the model as simple as possible but also detailed enough to describe phenomena of interest with some accuracy. Although the model might appear oversimplified or even artificial, it gives a very good description of characteristics of a remarkably wide variety of experimentally observable features related to the common *configuration mobilities* on the level of LITs. Moreover, it helps to identify the specific structural parameters to which the behavior is sensitive.

In the present paper we give the basic formulation of the model, including details of the simulation technique, which are described in section 2 and in the appendices. We discuss also a set of results of a numerical simulation of plastic flow in an ordered 2D solid at different temperatures and under different loading conditions. In the accompanying papers (II and III) we consider the equilibrium and relaxational properties of a model solid, including processes of ordering and disordering, undercooling and structural recovery (II), and features of plastic flow in ordered (crystalline) and disordered (glassy) solids (III).

2. Formulation of the model. Details of the numerical simulation

We consider below a 2D homogeneous isotropic linear elastic medium. We then arbitrarily tessellate the 2D plane into hexagonal elements, which form a regular 2D hexagonal lattice as shown in figure 1(*a*). We point out here that apart from certain rate properties that these volume elements will be endowed with, implying a length scale in the range of atomic dimensions, we do not presently associate the scales of our hexagons with any microstructural length scale. It is assumed further that under an applied external stress σ_{ij}, along with a uniform elastic response of the whole body, each of the hexagonal elements has several options to respond to the applied stress *inelastically*, so that it can spontaneously undergo one of six possible LITs, each characterized by its *eigenstrain tensor*‡ $\Delta e^{\mathrm{T}}_{ij}$ [6].

The hexagonal tessellation is chosen here, because hexagons have the highest symmetry with respect to other possible tessellations of the 2D plane in regular polygons—i.e., triangular and square lattices. It is sufficient to define a set of allowed inelastic transformations with symmetry properties not lower than the symmetry of the hexagonal lattice. The set of six transformations—three incremental elongations and three contractions along the symmetry axes of the lattice—is a reasonable choice that will permit development of the required response characteristics. Also, in order to keep the unconstrained volume (area) of the transforming element unchanged, the corresponding changes in transverse directions are necessarily assumed (figure 1(*b*)). For instance, for LITs numbers 1 and 4 the eigenstrains are given as

$$\Delta e^{\mathrm{T}}_{ij}(1) = 2e^{*}_{\mathrm{s}} \begin{pmatrix} 1 & 0 \\ 0 & -1 \end{pmatrix} \qquad \Delta e^{\mathrm{T}}_{ij}(4) = -\Delta e^{\mathrm{T}}_{ij}(1) \tag{1}$$

† In principle, the approach may be naturally extended to consider the inelastic response of a plastic material at arbitrarily large length scales and time intervals.

‡ Alternatively stated as the unconstrained transformation strain tensor, which describes the shape increment of the inelastic transformation when it occurs in the absence of an elastic surrounding.

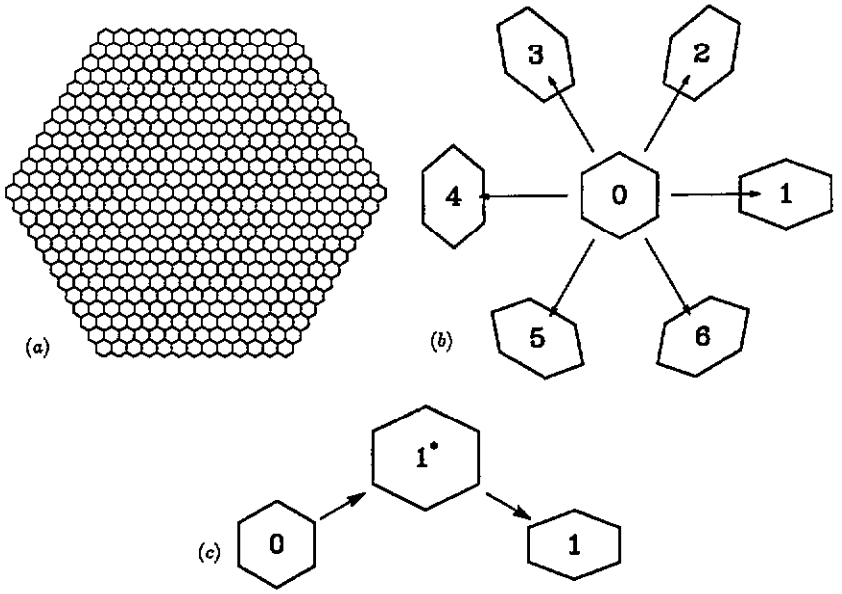

Figure 1. (*a*) A representative portion of the hexagonal tessellation. (*b*) The complete set of six possible plastic transformations. (*c*) In order to undergo a shear transformation (here of type 1) a hexagonal lattice element should acquire a certain transient dilatation in the intermediate 'on-barrier' configuration.

where $2e_s^*$ is the amplitude of inelastic transformations, which are all assumed to be of *pure shear type*, and where the 1 and 2 axes of the plane are toward the right and toward the top, as is conventional.

In order to be able to develop steady-state plastic flow under constant stress or constant-strain-rate loading conditions elements of the hexagonal mesh that are transformed once are allowed to undergo still further transformations, but from the same basis set of six incremental LITs. In other words, the magnitude of the plastic strain in a given element is assumed to have no bounds, other than distortion stresses, that must be accounted for to keep neighboring elements in reasonably close transformation states.

The probabilities of LITs developing per unit of time are defined in the framework of transition-state theory [7] as follows:

$$w = \omega_0 \exp\left[-\Delta G^*(\sigma)/kT\right] \tag{2}$$

where $\Delta G^*(\sigma)$ is the stress dependent (Gibbs) free energy barrier for inelastic rearrangement, k is Boltzmann's constant, T is the absolute temperature and ω_0 is the pre-exponential factor, characterizing the frequency of a normal mode leading to an unstable saddle-point configuration that has to be passed over on the way from the initial to the final (transformed) configuration.

In order to find $\Delta G^*(\sigma)$ we have to define shape increments Δe_{ij}^* of the hexagonal elements in the 'on-barrier' configuration. We describe these as follows (for the two generic cases 1 and 4):

$$\Delta e_{ij}^*(1) = e_s^* \begin{pmatrix} 1 & 0 \\ 0 & -1 \end{pmatrix} + e_d^* \begin{pmatrix} 1 & 0 \\ 0 & 1 \end{pmatrix} \qquad \Delta e_{ij}^*(4) = -e_s^* \begin{pmatrix} 1 & 0 \\ 0 & -1 \end{pmatrix} + e_d^* \begin{pmatrix} 1 & 0 \\ 0 & 1 \end{pmatrix}, \cdots, \tag{3}$$

where e_d^* is the transient volume (area) increment (dilatation in 3D), which is assumed to be the same for all six possible LITs. The last equations assign shape increments of different LITs in the transitional (dilatation) configurations to be half of the shear amplitude of the corresponding fully transformed states, with an additional dilatational component e_d^* (figure 1(*c*))†.

By introducing the latter coupled dilatational response we will account for the fact that in most cases inelastic shear rearrangements of atoms or molecules in densely packed structures require a local dilatation to permit the shear rearrangements to take place, and therefore necessitate overcoming strong repulsive forces acting between neighboring atoms.

The free-energy barrier in the limit of $\sigma \to 0$ may be written as

$$\Delta G^*(\sigma_{ij}) = \Delta F_0^* - \Omega \sigma_{ij} \Delta e_{ij}^*. \tag{4}$$

Here, ΔF_0^* is the (Helmholtz) free-energy barrier, which a transforming element would have to overcome in the absence of applied stresses $\Delta F_0^* = \Delta F^*(\sigma = 0)$, and the second term in (4) represents the work done by the stress imposed on the transforming element, which has an initial unperturbed volume Ω and acquires a transitory strain increment Δe_{ij}^* ‡.

It is important to note that the stress-dependent activation barrier (4) will be calculated using not the external stress σ_{ij}, but prevailing local stresses $\sigma_{ij}^{\text{local}}$, which are related to each other by the following expressions:

$$\sigma_{ij}^{\text{local}} = \sigma_{ij} + \sigma_{ij}^{\text{internal}} \qquad \langle \sigma_{ij}^{\text{local}} \rangle_V = \sigma_{ij} \qquad \langle \sigma_{ij}^{\text{internal}} \rangle_V = 0. \tag{5}$$

Here, angular brackets denote averaging over the entire volume V of the body, and internal stresses $\sigma_{ij}^{\text{internal}}$ originate form the elastic resistance of the matrix, which has to accommodate all the previously transformed elements, if there are any.

Using the method of Eshelby [8] for the plane strain state, it is possible to always obtain a general solution for the internal stress field in a linear elastic body due to arbitrarily distributed eigenstrains. It is useful then to obtain the 'lattice' Green tensor **X** [9]§, which is defined through the stress components (ij) averaged over a volume element with lattice index vector n_2 due to unit eigenstrain increment (kl) in an element with lattice index vector n_1 (here, lattice index vector n denotes the pair of indices enumerating elements of the hexagonal mesh). This gives, as explained in appendix A

$$\langle \sigma_{ij}^{\text{internal}}(n_2) \rangle_\Omega = X_{ijkl}(n_2 - n_1) e_{kl}^{\text{T}}(n_1). \tag{6}$$

Using equation (6) is crucial for the model in which we consider plastic deformation as a stochastic sequence of LITs with formation probabilities defined by (2), (3), and (4), and where internal stresses are being updated using (1) and (6), after each LIT.

In the numerical evaluations in the simulations a hexagonal simulation cell (figure 1(*a*)) containing 10 000 hexagonal elements was used, each capable of undergoing six possible LITs. Thus, the total number of possible outcomes at each step of the stochastic sequence was 60 000.

† We note that an activated-state dilatancy of the order of unity was actually observed for a sheared Bragg, soap-bubble-raft model by Argon and Shi [14].

‡ We note here that ΔF is usually shear dependent itself, and thus this must be considered if smooth behavior all the way to the mechanical threshold is desired. Nevertheless, here we develop only the customary linearized behavior.

§ We use the designation 'lattice' here to refer to the hexagonal unit cells into which the 2D space is divided. We still do not relate our developments to a real crystal lattice.

Two types of boundary condition were used: periodic continuation and one with a 'dead matrix with buffer zone'. The latter technique was specially designed in order to avoid physically unsound periodicity imposed on the system when periodic boundary conditions are used. To reduce undesirable influences of the rigid (dead) matrix outside the simulation cell, i.e., the build-up of the misfit stresses along the boundary, and, especially, in the corners, an additional hexagonal boundary zone was introduced dividing the simulation field in two regions—the central (core) and the peripheral (buffer). During numerical simulations the mean stress was kept at some specific level only in the core zone, with elements in the buffer zone being correspondingly adjusted. Most of the simulations were performed using boundary conditions of the second type.

Since macroscopic plastic flow is viewed here as a net result of the individual microscopic plastic events, it may be modeled if an appropriate *Markovian stochastic process* is defined. We shall specify a given state of the system by the corresponding set of accumulated plastic strain increments in each one of 10 000 lattice elements, or, equivalently, by the system's configuration. Any given configuration is assumed to have 60 000 different possibilities to change, and in order to fully characterize such a stochastic process it is sufficient to provide all 60 000 transition rates as functions of the current state.

These rates are given by the transition-state theory of (2) which, together with equations of the type (3), and making use of (4) and (6), may be rewritten as follows:

$$w(\boldsymbol{n}, \alpha) = \omega_0 \exp\left\{-\left[\Delta F_0 - \Omega\langle\sigma_{ij}(\boldsymbol{n}, t)\rangle e^*_{ij}(\alpha)\right]/kT\right\}. \tag{7}$$

Here $\boldsymbol{n}$ is the lattice index vector of a particular lattice element, and $\alpha = 1, 2, 3, 4, 5, 6$ enumerates plastic transformations of the six possible types.

The total rate for a transition into any other state, which determines the overall probability per time unit for the current configuration to transform, is the sum of all 60 000 transition rates, i.e.

$$w^{\text{total}} = \sum_{\boldsymbol{n} \in \text{lattice}} \sum_{\alpha=1}^{6} w(\boldsymbol{n}, \alpha). \tag{8}$$

This quantity defines the cumulative distribution of the time interval τ before the next transition takes place as

$$P(\tau) = 1 - \exp\left(-w^{\text{total}}\tau\right). \tag{9}$$

Therefore the residence time in a current configuration can be chosen according to the relation

$$\Delta t = -\ln(\xi)/w^{\text{total}}(t) \tag{10}$$

where ξ is a random number uniformly distributed in the interval [0,1). After this choice is made it is necessary to decide which particular element undergoes a transformation at this particular step, and on the particular type of transformation in that element. This decision is made according to the contributions of each individual transition to the total rate w^{total}, so that a subinterval of the width η is assigned for each of 60 000 possible transformations:

$$\eta(\boldsymbol{n}, \alpha) = w(\boldsymbol{n}, \alpha)/w^{\text{total}} \qquad \sum_{\boldsymbol{n} \in \text{lattice}} \sum_{\alpha=1}^{6} \eta(\boldsymbol{n}, \alpha) = 1. \tag{11}$$

Another random number ξ_2, uniformly distributed in the interval [0,1), is sufficient to choose the type and location of the next transformation.

Equations (8)–(11) fully specify the variant of the dynamic Monte Carlo (MC) method first introduced by Bortz and co-workers [10] that was employed here for simulations of plastic flow in the simple model proposed in this section. The overall procedure may be summarized as follows:

(i) for a given current configuration all 60 000 transition rates are computed according to equation (7);

(ii) the residence time and the type and location of the next transformation are randomly chosen according to (10) and (11);

(iii) the stresses on each of the 10 000 hexagonal elements are updated using equation (6); and

(iv) the procedure is repeated over and over by re-starting at step (i).

During the course of the MC simulations a record was kept of the primary information needed to specify the stochastic process of plastic flow, i.e., the time intervals between subsequent LITs, and the coordinates and types of subsequent LITs. Then these primary data were processed in order to obtain other characteristics of plastic response: average accumulated plastic strain, internal elastic energy, distribution of internal stresses, various correlation functions, etc. The records of primary data were also used as input information for graphical application programs, which were developed to visualize the evolution of the features of plastic flow structure in the simulation cell.

The use of the pre-tabulated lattice Green tensor given by (6) and vectorization of the computer code substantially increased the efficiency of computations, so that it required about 1 h of a single processor unit of an Alliant FX/8 computer to simulate a sequence of 20 000 LITs. The developed code was flexible enough to give inelastic responses of the model solid at temperatures and external stresses (or average total strains) that could be arbitrarily changed in time under specified stress (strain)–temperature–time programs. Moreover, it was possible to switch from one boundary condition to another in order to check the influence on the results of the rigid matrix approach or of the approach using periodic boundary conditions.

Below we list the model parameters required to specify a model elasto-plastic solid (material parameters) and the external conditions in which it is immersed.

(i) Material constants:

ω_0 - frequency factor,
Ω - area of hexagonal elements,
μ - shear modulus,
ν - Poisson's ratio,
e_s^* - shear strain increment on activation barrier,
e_d^* - inelastic dilatation increment on activation barrier, and
ΔF_0^* - the free-energy barrier at zero stress.

(ii) External parameters:

T - temperature,
σ_{ij} - external (average) stress tensor; or
ϵ_{ij} - external (average) total strain tensor.

Throughout the simulations the following basic units were used:

unit of time, $\tau_0 = \omega_0^{-1}$,

unit of length, $r_0 = \Omega^{1/2}$,
unit of energy, $E_0 = \mu r_0^3 (e_s^*)^2$, and
unit of 2D stress, $\pi = E_0/(r_0^2 e_s^*) = \mu r_0 e_s^*$.

3. Results and discussion

In this section we present some results of numerical simulations performed for the model solid with the following set of material constants†:

$\nu = 0.25$,
$e_s^* = 0.289$,
$e_d^* = 0.135$, and
$\Delta F_0^* = 0.115$ (in units of E_0).

Initially all hexagonal elements were chosen to be in an untransformed 'ground' state. Then some constant temperature and constant external stress of a certain type (isothermal creep regime) was specified and a stochastic sequence of LITs was started, with probabilities defined as explained in the previous section. With each new LIT occurring in the simulation all the internal elastic fields were recalculated. Therefore, even though the average stress was kept constant, the total internal stress distribution evolved with time. At a non-zero average stress, probabilities of different LITs were biased so that a non-zero plastic strain e_{ij}^p was produced. The latter was calculated as the sum of all plastic strain increments accumulated up to a current time, divided by 10000.

3.1. High-temperature flow

Shown in figure 2 are the longitudinal (11-component) and transverse (12-component) accumulated plastic strains calculated from the simulation data obtained at a constant temperature of $kT = 2.0$ and constant average stress of *pure shear type* with the following make-up‡:

$$\sigma = \sigma_s \begin{pmatrix} 1 & 0 \\ 0 & -1 \end{pmatrix} \qquad \sigma_s = 1.0. \tag{12}$$

As was expected the transverse component shows virtually no flow but only subtle fluctuations around zero strain rate, but the longitudinal plastic strain rate is non-zero and remains almost constant during the entire deformation process.

Taking advantage of the fact that we do have a well defined Markovian stochastic process we can compute independently the expectation value for the plastic strain rate for any current configuration, which is

$$\frac{de_{ij}^p}{dt} = \frac{1}{10^4} \sum_{\alpha=1}^{6} \sum_{n} w(n, \alpha) \Delta e_{ij}^T(\alpha) \tag{13}$$

† The material constants were chosen to match those obtained for a 2D simple atomic model studied in [2] (see also II). All the results presented in the present paper are in the scaled units.

‡ Unrealistically high values of the applied stress appearing throughout the paper are due to the particular choice of the basic units. In order to obtain all the results in more acceptable magnitudes of stress measured as a fraction of the shear modulus μ it is sufficient simply to multiply all the stresses by the factor e_s^*, which is expected to be in the range from 0.01 to 0.2 [5].

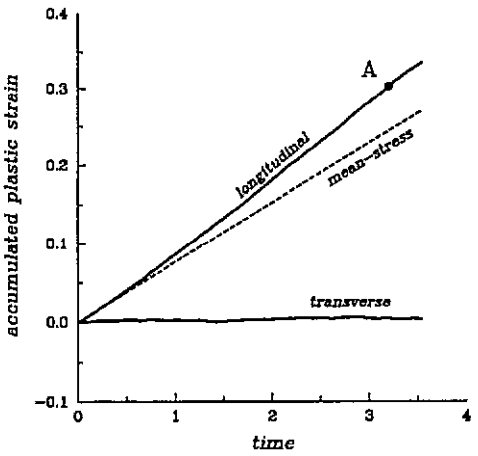

Figure 2. Accumulated plastic strain as a function of time for the high-temperature—high-stress creep simulation ($kT = 2.0$, $\sigma_s = 1.0$, initial state = 'no LITS').

where $\Delta e_{ij}^{T}(\alpha)$ is the α-type transformation strain increment and $w(n, \alpha)$ is the probability per unit time for this transformation to happen in the lattice element n. If we now combine equation (12) with equations (1)–(4), we obtain

$$\frac{de_{ij}^{p}}{dt} = \frac{\omega_0}{10^4} \exp\left(\frac{-\Delta F_0}{kT}\right) \sum_{n} \exp\left(\frac{\Omega e_d^* \sigma(n)}{kT}\right) \sum_{\alpha=1}^{3} 2\Delta e_{ij}^{T}(\alpha) \sinh\left(\frac{\Omega \Delta e_{kl}^{T}(\alpha) s_{kl}(n)}{2kT}\right) \quad (14)$$

where $\sigma(n)$ $(= \sigma_{11}(n) + \sigma_{22}(n))$ is the trace and $s_{ij}(n)$ $(= \sigma_{ij}(n) - \delta_{ij}\sigma(n)/2)$ is the traceless part of the 2D stress tensor averaged over lattice element n.

Equation (14), if taken by itself, does not simplify our considerations, since, in order to actually calculate the expectation value of plastic strain rate, it is necessary to know the stresses in all 10 000 lattice elements. However, the value of plastic strain rate may be calculated in the mean-stress approximation which is expected to give a reasonable description of plastic flow at high temperatures where stress fluctuations may be neglected. In the mean-stress approximation it is assumed that each lattice element sees a mean stress field due to its neighbors and an external stress field. According to equation (5) mean stress is equal to the applied stress σ_{ij}, therefore in this approximation equation (14), for the special case $\sigma_{11} = \sigma_{22}$, can be reduced to a simpler form

$$\frac{de_{11}^{p}}{dt} = \omega(T) \sum_{\alpha=1}^{3} \Delta e_{11}^{T}(\alpha) 2 \sinh\left(\frac{\Omega \Delta e_{11}^{T}(\alpha) \sigma_s}{kT}\right) \quad (15)$$

where $\omega(T) = \omega_0 \exp(\Delta F_0/kT)$ is the stress-independent factor and σ_s is the non-zero shear component of the applied stress. The mean-stress expectation value of accumulated plastic strain computed using equation (15) is plotted in figure 2 as the dashed line, and it agrees well with the simulation result. This shows that plastic flow at $kT = 2.0$ and $\sigma_s = 1.0$ may be reasonably described on the basis of the mean-stress approximation†.

† Deviation of the simulated and the mean-stress curves in figure 2 is apparently due to the fact that even at such a high temperature the plastic strain field developing under applied stress is not totally uncorrelated.

To observe the detailed evolution of plastic strain on the level of individual hexagonal elements a graphical representation scheme was developed, where each LIT was represented as an increment in color intensity of the corresponding element, properly positioned at monitor screen field. Time intervals between inelastic events were chosen to be proportional to the corresponding time increments in the simulations.

With properly adjusted playback rate it was possible to observe a graphical representation of the consecutive development of colorful configurations of local plastic fields. Shown in figure 3 is a black and white copy of a typical configuration of inelastically transformed elements for an instant of time marked A in figure 2. Untransformed elements are shown there as white, but those, that have positive longitudinal plastic strain increments—i.e., extended along the horizontal axis—are shown in different shades of gray, depending on the amplitude of accumulated inelastic strain in each particular element.

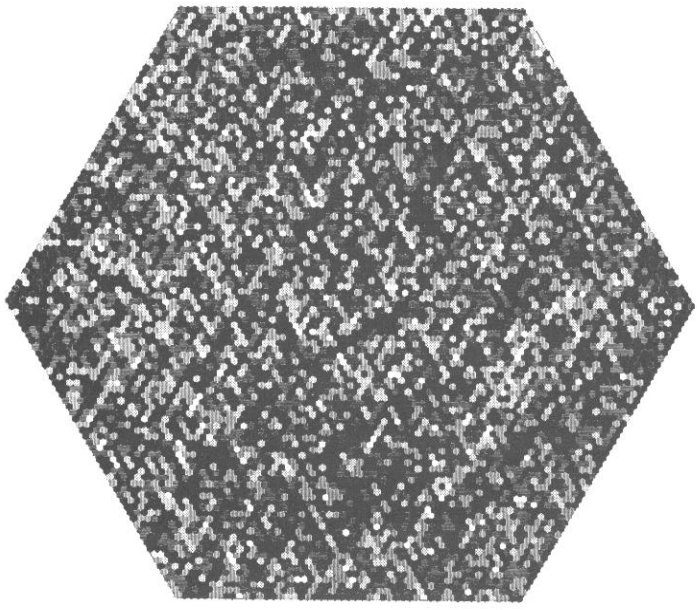

Figure 3. A typical configuration of the plastic strain field obtained for the high-temperature—high-stress creep simulation.

Figure 3 shows that plastic flow at such a high temperature is quite uniform (diffuse) in the sense that there are no significant spatial correlations in local plastic strain intensity, or, in other words, the structural correlation length [11] is much smaller than the simulation cell dimension.

The development of both longitudinal and transverse plastic strains at smaller applied stress $\sigma_s = 0.1$ but at the same high temperature $kT = 2.0$ is shown in figure 4. The dashed line again represents the corresponding mean-stress value for the longitudinal plastic strain calculated with equation (15). This figure also confirms that the mean-stress approximation works well enough at high temperatures, where correlations are weak and may be neglected. Parenthetically, the ratio of average plastic strain rates for the two levels of applied stress differing by a factor of 10 was found to be 11.3. This shows that at such a high temperature our model solid exhibits nearly *Newtonian flow*, characteristic of liquids.

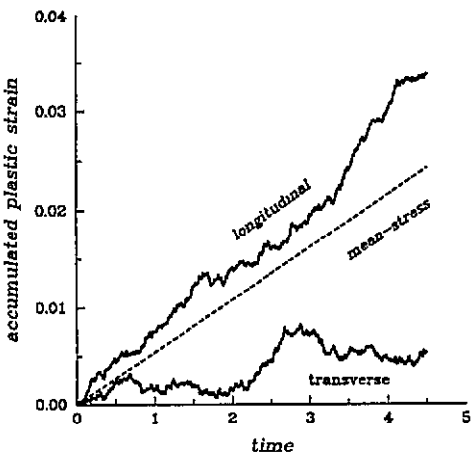

Figure 4. Accumulated plastic strain as a function of time for the high-temperature—low-stress creep simulation ($kT = 2.0, \sigma_s = 0.1$, initial state = 'no LITs').

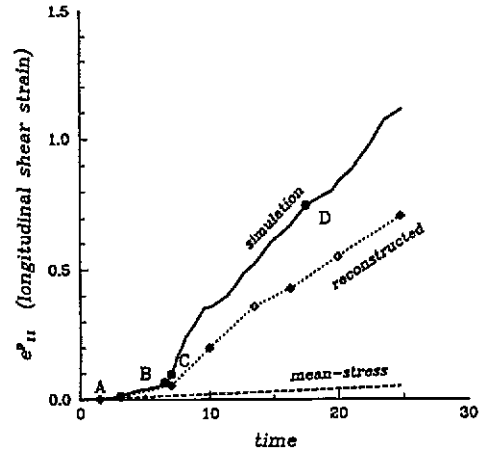

Figure 5. Accumulated longitudinal plastic strain as a function of time for the low-temperature—high-stress flow simulation ($kT = 0.15, \sigma_s = 1.0$, initial state = 'no LITs').

3.2. *Low-temperature creep. Plastic strain localization*

Simulations of isothermal creep response of initially ordered material performed at the same low stress $\sigma_s = 0.1$ but at substantially lower temperature $kT = 0.15$ showed no plastic response at all for reasonably long runs (up to times of the order of 10^7 accumulated LITs). The reason for this behavior was that there was not more than one LIT at a time present in the entire simulation cell, and it always disappeared very quickly after having been produced. This demonstrates that some critical shear stress is necessary to initiate stable plastic flow at such a low temperature in the initially perfectly ordered solid, and that the residual stresses around the LIT nearly always transform it back under such low stress.

Application of higher stress $\sigma_s = 1.0$ at the same low temperature, however, produces desirable flow, which is shown in figure 5 in terms of longitudinal plastic strain rate as a function of time. Along with a clear transition from a nearly no-flow-type response characteristic of low-stress behavior to quite a substantial plastic flow rate at higher stress, another characteristic feature of the observed behavior is worth considering in detail. The initially relatively low plastic strain rate then increases dramatically, about 20-fold, in a very narrow time interval. Both the threshold-like behavior and the apparent change of flow mechanisms observed in low-temperature creep simulations may be explained if the energetics of LITs in our model solid are considered in more detail. Below we discuss these effects based on a simple semi-quantitative analysis of a few important states of the model solid, and compare the predictions of such an analysis with results obtained in the numerical simulations.

First, we note that the zero-stress free-energy barrier ΔF_0^* (4) may be viewed as consisting of two parts having quite different physical meanings: an internal free-energy barrier for collective inelastic rearrangements of particles (atoms, molecules or molecular fragments) comprising the smallest irreducible elements of plastic flow, and an additional energy contribution due to the reaction of the elastic surroundings to a transformation occurring in the plastic core.

According to Eshelby [8] the total transformation strain energy in the matrix and the inclusion is

$$E_{\mathrm{el}} = -(\Omega/2)\langle\sigma_{ij}^{\mathrm{I}}\rangle e_{ij}^{\mathrm{T}} \tag{16}$$

when the transformation occurs under no external stress, where $\langle\sigma_{ij}^{\mathrm{I}}\rangle$ is the average over the inclusion volume Ω of a backstress exerted by the surrounding matrix on the inclusion, and e_{ij}^{T} is a transformation strain, which is assumed here to be uniform in the inclusion volume. This can also be written as

$$E_{\mathrm{el}} = -(\Omega/2)X_{ijkl}(0)e_{ij}^{\mathrm{T}}e_{kl}^{\mathrm{T}} \tag{17}$$

where $X_{ijkl}(0)$ is the central, 'unshifted' value of the 'lattice' Green tensor of equation (6). After substitution of the 'on-barrier' transformation strain, as defined by equation (3), for e_{ij}^{T} in the last equation we obtain for LIT number 1

$$\begin{aligned} E_{\mathrm{el}}^{*} = -(\Omega/2)\big[&\big(X_{1111} + X_{2222}\big)\big(e_{\mathrm{d}}^{*2} + e_{\mathrm{s}}^{*2}\big) + 2X_{1122}\big(e_{\mathrm{d}}^{*2} + e_{\mathrm{s}}^{*2}\big) \\ &+ 2\big(X_{1111} - X_{2222}\big)e_{\mathrm{d}}^{*2}e_{\mathrm{s}}^{*2}\big]. \end{aligned} \tag{18}$$

The last term in square brackets would be zero, if the shape of the transforming element were round. In fact, it is non-zero for a hexagonal element. However, more detailed calculations show that the last term is still an order of magnitude smaller than the first two terms in square brackets. Therefore, neglecting the last term we obtain the elastic contribution to the activation barrier (due to the internal backstresses), as the sum of a dilatational and a shear contribution

$$\Delta F_0^{*\,\mathrm{elastic}} = ae_{\mathrm{d}}^{*2} + be_{\mathrm{s}}^{*2} \tag{19}$$

where a and b are two numerical factors, depending on the shape of inclusions, which are both positive and of the order of unity. Consider now energies for three different states of our model solid. The energy is

(i) zero for the initial untransformed configuration,
(ii) $4b(e_{\mathrm{s}}^{*})^2$ for a configuration with only one element transformed, and
(iii) $\Delta F_0^{*\mathrm{intrinsic}} + a(e_{\mathrm{d}}^{*})^2 + b(e_{\mathrm{s}}^{*})^2$ when the transforming element is on the top of the potential barrier.

This allows us to compare the transition rate for the initially untransformed state into state number 1, which contains only one isolated transformation of, say, type 1, with the rate for the reverse transformation in the case when an external stress of the type given by equation (12) and an amplitude σ_{s} is applied

$$w(0 \to 1)/w(1 \to 0) = \exp\big[\big(2\sigma_{\mathrm{s}}e_{\mathrm{s}}^{*} - 3be_{\mathrm{s}}^{*2}\big)/kT\big]. \tag{20}$$

According to the last equation two distinct types of response may be expected depending on the magnitude of the stress applied to the initially untransformed configuration.

(i) If $\sigma_{\mathrm{s}} < 3be_{\mathrm{s}}^{*}/2$, the ratio (20) is smaller than unity. This implies that, after a transformation occurs in one of the 'lattice' elements, the transformed element immediately transforms back to recover its initial untransformed shape. Behavior of such a kind was indeed observed at low temperature $kT = 0.15$ and low applied stress $\sigma_{\mathrm{s}} = 0.1$.

(ii) If $\sigma_{\mathrm{s}} > 3be_{\mathrm{s}}^{*}/2$, then the ratio (20) is of an order in excess of unity, which means that the system resides in a transformed state for a time interval long enough that some more transformations may be produced before the first transformed element recovers its initial

state. Therefore, at a higher applied stress one may expect that an observable plastic flow process can be produced.

The sharpness of this transition depends on temperature, ranging from the low-temperature case where an athermal shear threshold needs to be overcome at zero temperature, to a high-temperature situation discussed in the previous subsection, where hardly any transition could be observed.

Quite similar considerations, if applied to the energetics and the transition rates for the lattice elements surrounding a previously transformed one, allow for another qualitative conclusion. The probability that a further transformation occurs, giving rise to macroscopic plastic flow, is higher for some of the lattice elements having neighbors that have been previously transformed than for remote lattice elements. Such a difference is, of course, more likely at lower temperatures. Therefore, one should expect that the same model solid, which flows uniformly at high temperatures, may exhibit a strong shear localization at lower temperatures. This was indeed observed, as illustrated in figure 6 obtained for the following loading conditions: $\sigma_s = 1.0$, $kT = 0.15$.

Shown in figure 6 are four structures of LIT groups, each corresponding to different stages of flow marked A, B, C, and D in figure 5. While configuration A pertaining to the start-up process contains only a few LITs, more or less randomly distributed over the simulation cell, very soon several shear bands are nucleated and begin to grow (configuration B). After a short transient period a well developed shear band structure is observed (configuration C), and further flow is produced mostly by the involvement of increasingly more elements in the bands already formed. Then, shortly before the previously established shear bands expand through the whole volume, some new shear bands appear, and eventually an intensely banded steady state flow structure is established (configuration D). The dramatic increase of the flow rate, as shown in figure 5, is strongly related to the onset of shear localization. Initially, before shear bands appear, the plastic strain rate is close to what is expected from the mean-stress equation (15). However, as the first shear bands are formed the strain rate increases, which may be attributed to the stress concentration at the edges of shear bands, or stated differently, due to the development of a characteristic flow state of lower effective resistance that gives rise to the shear bands. Due to this effect the operating stress in the elements neighboring to shear bands may become significantly higher than the applied stress, and, therefore, the flow rate rises. Again, speaking in somewhat different terms, the observed increase in plastic strain rate is caused by changes in internal structure of the solid, which becomes very non-uniform with the first shear bands formed. Therefore, to provide a better description of plastic flow it is necessary to account for the evolution of structure (with its associated non-random internal stresses) in the course of deformation.

Apparently, at a very low temperature when shear band formation and growth is the predominant mechanism of plasticity, the evolving structure may be reasonably described by specifying positions, orientations, and lengths of all the shear bands present in the simulation volume. Here, however, we try to explore another possible choice of structural parameters, which appears to be more natural and operationally convenient for the present model. Basically, we shall try to describe the evolution of internal structure in terms of internal stress distribution, which reflects existing non-uniformities of the structure and directly determines the plastic strain rate through equation (14).

There are only three relevant components of the stress tensor in the 2D case considered here, which are, in fact, related to each other through a single compatibility equation [12]. It is not clear, however, how much this relationship affects the statistical parameters of internal stress distribution, which seems to show no correlations between different components of

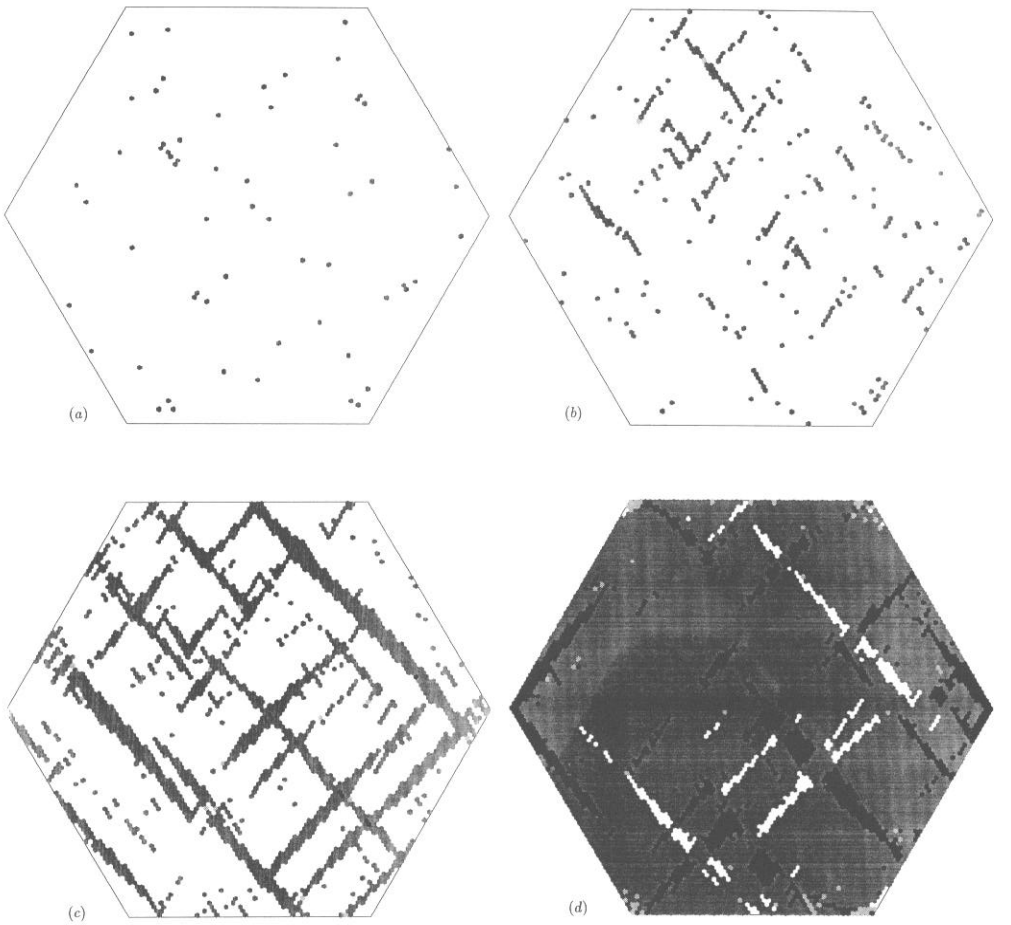

Figure 6. Time evolution of the plastic strain field configuration obtained for the low-temperature—high-stress simulation related to the history of figure 5: (*a*) the configuration corresponding to the point marked A in figure 5; (*b*) point B; (*c*) point C; (*d*) point D.

the internal stress tensor in the case of zero applied stress (see also II), but appears to be correlated when a non-zero external stress is applied and some plasticity is produced.

In figure 7 we show the evolution of the s_{11} component of internal stress distribution for the same four configurations as shown before in figure 5 and figure 6. Apparently the distribution broadens with time and becomes skew. Nevertheless, trying to keep our treatment simple, we assume that the distribution of internal stresses may be described as having a three-component Gaussian density function for the joint distribution of all three components of the internal stress tensor (an abbreviated notation for the components of the stress tensor commonly accepted for the plane strain analysis is used here, where $\sigma_1 = \sigma_{11}, \sigma_2 = \sigma_{22}, \sigma_3 = \sigma_{12}$),

$$\varphi(\sigma_1, \sigma_2, \sigma_3) = \frac{1}{[(2\pi)^3 \det(Q_{mn})]^{1/2}} \exp\left(-\tfrac{1}{2} \sum_m \sum_n Q^{-1}_{mn} \sigma_m \sigma_n\right) \tag{21}$$

$$Q_{mn} = \langle \sigma_m \sigma_n \rangle_V \qquad m, n = 1, 2, 3. \tag{22}$$

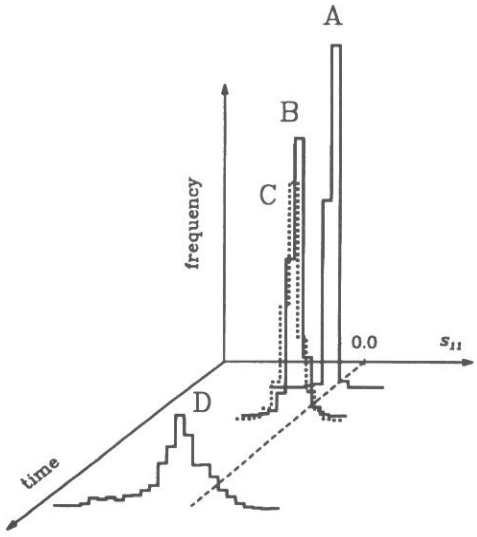

Figure 7. Time evolution of the internal stress distribution s_{11}.

Here, φ is the density function of internal stress distribution, Q_{mn} is the so-called covariance matrix, which has dispersions of the stress components on its diagonal, while its off-diagonal elements correspond to cross-correlations of different internal stress components. Q^{-1}_{mn} is the inverse of the covariance matrix [13]. The covariance matrix† itself may be considered as a structural parameter evolving with time, and for each instance of time may be obtained by averaging the corresponding bilinear combinations of stress components over the entire volume V.

In appendix B we derive an expression for the average expected plastic strain rate in the Gaussian approximation. Here we give only the final form of the equation, as

$$\frac{\mathrm{d}e^{\mathrm{p}}_{11}}{\mathrm{d}t} = \omega(T)\sum_{\alpha=1}^{3}\Delta e^{\mathrm{T}}_{11}(\alpha)2\,\sinh\left(\frac{\Omega\Delta e^{\mathrm{T}}_{11}(\alpha)\sigma_{\mathrm{s}}}{kT}\right)\gamma(\alpha) \tag{23}$$

where $\gamma(\alpha) = \langle\exp[\sum\Omega\Delta e^{*}_{i}(\alpha)\sigma^{\mathrm{internal}}_{i}/kT]\rangle$ are the factors that determine how much the (non-random) distribution of internal stress affects the rate of plastic flow. According to equation (B3) of appendix B the factors $\gamma(\alpha)$ may become very large if the distribution of internal stress is broad and/or the temperature is low. In the opposite limit of uniform stress and/or very high temperature these 'amplification factors' are all equal to unity and equation (23) is reduced to the mean-stress form (15).

In order to verify how well equation (23) describes the plastic strain rate in the case of inhomogeneous low-temperature flow we have computed matrix **Q** for several configurations encountered in the discussed simulation run. Then we reconstructed the plastic strain rate using equation (23). The results of such a reconstruction are shown as diamonds in figure 5. Clearly, in spite of the apparent non-Gaussian nature of the internal stress distribution, the approximation used here produces a qualitative description of the trend observed in the transition from initial non-correlated flow to localized flow in transient and steady-state regimes, except that the strain rate predicted by equation (23) is still somewhat lower than

† Note that the averages of internal stress components are all zero in the simulations discussed.

that obtained in the simulation. Actually, at even lower temperatures the description of plastic flow in an initially perfect solid given by equation (23) becomes rather poor due to the fact that in this case the internal stress distribution may not be considered even approximately to be Gaussian. Instead, along with the above mentioned skewness the distribution also shows two outstanding shoulders at its lower and higher ends which are due to an extreme stress concentration in the elements at and near the edges of shear bands. When such ultralocalized flow occurs the Gaussian approximation (23) becomes inadequate, although, even in such a case, it gives still a better description of the real kinetics than the mean-stress approximation of equation (15) may provide.

In general, our observations imply that a simplified description of the structure of plastically deformed solids in terms of the internal stress distribution is a very meaningful option for theoretical analysis. However, further work is needed in order to actually find equations governing the evolution of structural parameters, whatever they might be. We expect that the simple model discussed above will be helpful in at least the initiation of such a solution.

Finally, we note that in the past shear localization has been attributed primarily to a dilatancy-induced reduction of plastic resistance (see, e.g., [2]). Our model developed here demonstrates that while this is indeed likely, it is not the only cause of localization. Evolution of non-random internal stresses is at least as important.

4. Conclusions

The results of the simulations discussed above show that the model proposed here, in spite of its simplicity, describes some phenomenological aspects of the solid-state plasticity rather well. Among them is the widely encountered phenomenon of the transition from diffuse plastic flow at high temperatures to well localized flow through the shear bands at low temperatures.

In fact, the only principal assumption that the present model is based on is that plastic flow in solids may be considered to result from individual localized plastic transformations. However, the critical step in developing the model was the explicit accounting for the changes in the elastic stress field that accompany these individual plastic events. Such elastic interactions, being of sufficiently *long-range* character, are not fully accounted for in the mean-stress approximation commonly used for description of the solid-state plasticity. Instead, parameters of the internal stress distribution are shown to give a more detailed description of the kinetics of plastic flow, and, as is also important, influence the development of the familiar features of banded deformation.

The computational scheme discussed here allows for simulations of large-length-scale response of the model solid to arbitrary changes in external parameters—temperature and stress (or strain)—and corresponding structural metamorphoses, and will be explored further in the two accompanying papers II and III.

Acknowledgments

This research was supported by a DARPA/URI program through the ONR under contract N00014-86-K-0768. Salary support for VVB was provided from a special fellowship from the William and Mary Greve Foundation and from an Allied Signal Corporation fellowship for which we are grateful to Drs John Kiser and Lance Davis, respectively.

Appendix A

In order to obtain the necessary 'lattice' Green tensor needed in the numerical integration procedures that we will use we have reduced as far as possible the order of integrals that need to be handled.

Generally, it was necessary to calculate the average over the volume of element Ω_2 of the stress increment σ_{ij} produced by an inelastic transformation with an eigenstrain e^{T}_{ij}, which is assumed to be constant in the volume element Ω_1 (figure A1). In a uniform unbounded linear elastic body these two tensors are related as follows

$$\langle \sigma_{ij} \rangle_{\Omega_2} = X_{ijop}(R_{21}) e^{\mathrm{T}}_{op}$$

where **X** is a fourth-rank tensor, which was found to be

$$X_{ijop}(R_{21}) = \tfrac{1}{2} C_{ijkl} C_{mnop} \oint_{L_1} \mathrm{d}\zeta^{(1)}_n \oint_{L_2} [G_{km}(x_2 - x_1)\mathrm{d}\zeta^{(2)}_l + G_{lm}(x_2 - x_1)\mathrm{d}\zeta^{(2)}_k]. \qquad \text{(A1)}$$

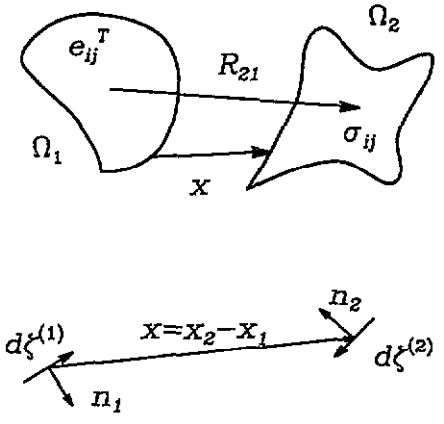

Figure A1. Calculations of the 'lattice' Green tensor.

Here, C_{ijkl} is the fourth-rank tensor of elastic constants, G_{ij} is the Green tensor for the plane strain state, which gives the displacement u_i at point x_2 due to the point force applied at point x_1, i.e.,

$$u_i = G_{ij}(x_2 - x_1) f_i$$

and becomes for the isotropic, plane strain state [6]

$$G_{ij}(x_2 - x_1) = -\left(\frac{1}{8\pi\mu(1-\nu)}\right)\left((3-4\nu)\delta_{ij}\log|x_2 - x_1| - \frac{(x_2 - x_1)_i (x_2 - x_1)_j}{(x_2 - x_1)^2}\right). \qquad \text{(A2)}$$

The relation (A1) was obtained by using Gauss's theorem to reduce the order of integration, which is performed here along two contours bounding volume elements Ω_1 and

Ω_2, and the contour elements $d\zeta_n^{(1)}$ and $d\zeta_j^{(2)}$ are the contour length increments multiplied by the corresponding normal vectors. The directions of contour integrations with respect to normals are also shown in figure A1. In spite of the substantially reduced number of calculations needed to obtain the 'lattice' Green tensor X formula (A1) could not be used for numerical integrations because of apparent divergence of the plane-strain Green function (A2) as $x_2 - x_1$ approaches zero.

To avoid this divergence problem we may consider only such contours as consist of straight segments, connected so as to form piecewise continuous closed contours, i.e., polygons. Now, the integrals in (A1) may be found by simple summation if they can be calculated for the case of two straight segments generally oriented with respect to each other and separated by an arbitrary vector x (figure A1). In this case all the integrals may be reduced to tabulated forms, and the apparent divergence is, of course, eliminated. However, we will not give here explicit results of such calculations, since they are very lengthy and would not add to overall clarity. In order to check the computer program, developed to handle all these tedious calculations, we compared stresses calculated for the interior of the circle with the exact solution given in [6]. Having thus established that the code is reliable, tensors X for two arbitrary regions, bounded by piecewise linear contours, separated by an arbitrary vector could be readily computed.

Such computations were performed for all possible lattice vectors, separating hexagonal elements of the simulation cell. The symmetry of the hexagonal lattice was used to reduce the number of different elements of such an array to about 120 000 for the cell of dimensions 100×100 (isotropic case).

Appendix B

In order to calculate the expected average plastic strain rate at a given distribution of internal stresses, which we assumed to be Gaussian, it is necessary to average with the density function (21) the stress-dependent plastic strain rate

$$\frac{de_{ij}^{p}}{dt} = \sum_{\alpha=1}^{6} \eta_{ij}(\alpha) \exp\left(\frac{\Omega \sigma_{i_1 j_1}^{\text{internal}} \Delta e_{i_1 j_1}^{*}(\alpha)}{kT}\right) \qquad \alpha = 1, 2, 3, 4, 5, 6 \tag{B1}$$

where tensors $\eta_{ij}(\alpha)$ depend solely on the external (average) stress tensor and temperature, but not on the internal stress tensor $\sigma_{ij}^{\text{internal}}$, and, therefore, need not be integrated. So, formally it is necessary to average over distribution (21) exponents containing linear forms of internal stress components, such as

$$\left\langle \exp\left(\sum_n a_n(\alpha)\sigma_n\right)\right\rangle = \frac{1}{\sqrt{(2\pi)^3 \det\{Q_{ij}\}}} \int \prod_k d\sigma_n \exp\left(-\tfrac{1}{2}\sum_{m,n} Q_{mn}^{-1}\sigma_m\sigma_n + \sum_n a_n(\alpha)\sigma_n\right)$$

$$k, n, m = 1, 2, 3 \qquad \alpha = 1, 2, 3, 4, 5, 6$$

where

$$a_n(\alpha) = \Omega \Delta e_n^{*}(\alpha)/kT \tag{B2}$$

and k, n, m are the single indexes commonly used for short-hand notation subscripts of the stress in the plane-strain problems. Now, if we rewrite the initial set of integration variables in another coordinate system, which is based on the eigenvectors of the bilinear form Q_{mn},

then the required integral may be readily found to be (no summation over repeated indexes is implied):

$$\langle \exp[a_n(\alpha)\sigma_n] \rangle = \exp\left[\frac{1}{2}\sum_k \lambda_k \left(\sum_l T_{kl} a_n(\alpha)\right)^2\right]. \tag{B3}$$

Here, T_{kl} is the matrix of rotation from the initial coordinate system to a new one, in which the covariance matrix Q_{mn} is now diagonal, and λ_1, λ_2, and λ_3 are the eigenvalues of **Q**. The latter and the transformation matrix T_{mn} may be found using appropriate numerical procedures. The last thing that needs specifying now is the tensors $\eta_{ij}(\alpha)$, which are

$$\eta_{ij}(\alpha) = \omega_0 \Delta e_{ij}^{\mathrm{T}}(\alpha) \exp\left\{-\left[\Delta F_0 - \Omega \sigma_{ij}^{\text{external}} \Delta e_{ij}^{*}(\alpha)\right]/kT\right\}. \tag{B4}$$

Formulae (B1)–(B4) give a complete description of the procedure that was used to calculate the average expected plastic strain rate in the Gaussian approximation.

References

[1] Maeda K and Takeuchi S 1982 *J. Phys. F: Met. Phys.* **12** 2767
Srolovitz D, Vitek V and Egami T 1983 *Acta Metall.* **31** 335
[2] Deng D, Argon A S and Yip S 1989 *Phil. Trans. R. Soc.* A **329** 613
[3] Kotelyanskii M J, Mazo M A, Oleynik E F and Grivtsov A G 1001 *Phys. Status Solidi* b **166** 25
[4] Hutnik M, Gentile F T, Ludovice P J, Suter U W and Argon A S 1991 *Macromolecules* **24** 5962
[5] Mott P, Argon A S and Suter U W 1993 *Phil. Mag.* **67** 931
[6] Mura T 1987 *Micromechanics of Defects in Solids* (Dordrecht: Martinus Nijhoff) p 2
[7] Halsey G, White H J and Eyring H 1945 *Text Res. J.* **15** 295
[8] Eshelby J D 1957 *Proc. R. Soc.* **241** 376
[9] Teodosiu C 1982 *Elastic Models of Crystal Defects* (Berlin: Springer) p 260
[10] Bortz A B, Kalos M H and Lebowitz J L 1975 *J. Comput. Phys.* **17** 10
[11] Ziman J M 1979 *Models of Disorder* (Cambridge: Cambridge University Press) p 57
[12] Timoshenko S and Goodier J N 1951 *Theory of Elasticity* (New York: McGraw-Hill) p 229
[13] Devore J L 1982 *Probability and Statistics for Engineering and the Sciences* (Monterey, CA: Brooks–Cole) p 181
[14] Argon A S and Shi L T 1983 *Acta Metall.* **31** 499

Modelling Simul. Mater. Sci. Eng. 2 (1994) 185–202. Printed in the UK

A stochastic model for continuum elasto-plastic behavior: II. A study of the glass transition and structural relaxation

V V Bulatov† and A S Argon
Massachusetts Institute of Technology, Cambridge, MA 02139, USA

Received 26 January 1993, accepted for publication 3 August 1993

Abstract. The numerical approach, proposed by us in an associated paper, is further developed here to account for the processes of ordering and disordering in a 2D idealized elasto-plastic body. Study of the kinetic and structural aspects of such processes reveals various features characteristic of the glass transition and structural relaxations in real glasses. Results of numerical simulations and the relative glass-forming ability of liquids are discussed in terms of geometric and energetic parameters of local inelastic processes. Methods of obtaining and analyzing undercooled structures with controlled degrees of frozen-in disorder are developed.

1. Introduction

The plastic response of disordered solids is known to depend strongly on their packing structure. It is not surprising, therefore, that much effort has been directed so far to establish reliable interrelations between structure and plasticity in disordered solids, and in glasses in particular. Another important issue, which is often addressed in the literature, is how conditions at which glasses are formed or treated affect their structure and, hence, plastic properties [2].

It is highly desirable to analyze all the above-mentioned problems on a common basis, and this is our primary concern in the present series of papers of which this is the second. In the preceding paper [1] (hereafter referred to as I) a numerical model was introduced for describing a certain type of plastic flow in solids that is initiation controlled. In this model macroscopic plasticity was treated as a net result of local inelastic rearrangements in small volume elements that can be interpreted as involving a few atoms or molecular groups. It was shown that various aspects of solid-state plasticity, particularly of amorphous media, were well reproduced in the model, including the transition from uniform plastic flow at high temperatures to highly localized flow at low temperatures.

In the present paper the same model is used to consider the most important features of the glass transition and structural relaxations in amorphous media, but no attempt is made to develop all the potentials of the model in detail. Instead, the primary target here is to develop a means for obtaining and analyzing undercooled disordered structures stable enough to be subjected later to mechanical loading. Therefore, the present work should be viewed as preparatory for further studies of plasticity in disordered solids, which are to be discussed in greater detail in the third paper of this series [3], referred hereafter to as III. However, it is intended that the results reported below stand on their own and will

† On leave from the Institute of Chemical Physics, Russian Academy of Sciences, Moscow, Russia.

0965-0393/94/020185+18$19.50

contribute to better understanding of the glass transition and structural relaxation processes in atomic (non-bonded) glasses.

In what follows, attention is focused mostly on two important aspects of the glass transition: the ability of a melt to vitrify [4] and the apparent *multi-modality of structural relaxation* in the glass-transition region [5].

In general, the ability of a liquid with a certain chemical composition to be undercooled and to form a glass is related to the presence in it of some slowly relaxing degrees of freedom, which may be frozen out if appropriate cooling conditions are chosen [4]. In a polymeric glass such sluggish degrees of freedom may be attributed to very slow motions of polymer chains in the melt, constrained by various topological obstacles such as chemical crosslinks, entanglements, loops, etc [6], not to mention the need to reptate a molecule through a representative environment to create order. In silicate glasses slow-relaxing degrees of freedom may be related to covalent bonds connecting constituent atoms to form *a covalent bond network* [7]. Probably the most important source of glass-forming ability for metal alloys is the compositional disorder, which requires a substantial length of time to relax on its way to the required, energetically favorable phase-separated structure [8].

All the above-mentioned motions have at least one feature in common: they are most likely to be accomplished via more or less localized inelastic rearrangements. Although length scales, topology, geometry and energetics of such transformations may vary substantially† it is the localized character of such rearrangements that the present model tries to exploit. The applicability of such an approach is justified, among other things, by the observed universality of phenomenology of both the glass transition and plasticity in disordered solids of different composition and structural make-up, and, as is discussed below, even in a very simple model it is possible to obtain undercooled structures mimicking certain characteristics of real glasses.

Another important issue is the apparent multi-modality of structural relaxations as it has been extensively discussed in the literature starting with Kohlrausch [25] and more recently developed by Kovacs [5] in relation to polymeric glasses. It was shown very clearly by these extensive studies that the kinetics of structural relaxation in the glassy region up to and including the glass transition cannot be described with a single relaxing parameter, indicating the intrinsic multi-modality of the relaxation process. The latter has been interpreted in many different ways reviewed recently by Johari [11]. Our present development will shed a different light on this complex process and will sharpen the perspective on the processes that are involved.

2. Details of simulations. Equilibrium properties of a model solid

The model introduced and discussed in detail in I is based on the assumption that local inelastic rearrangements of atoms or molecular groups constitute the type of *configurational mobility* solely responsible for plastic flow. We will discuss here the fact that it also applies to other macroscopically observable phenomena such as structural relaxation, and vitrification. In order to keep the model simple, but still capable of coping with the most important aspects of the phenomena of interest, a 2D homogeneous isotropic linear elastic body arbitrarily tessellated into a regular hexagonal mesh is considered‡. Each hexagonal

† Results of atomic-level simulations show that the characteristic scales of the cooperative inelastic transformations in polymeric glasses [9] are much larger than those observed for simple atomic models [10].

‡ While the hexagonal mesh conveniently defines a structural unit of independent relaxation properties, we leave the association with any specific atomic process open. When we refer to the mesh as a 'lattice' it is only because of its symmetry properties.

element is allowed to spontaneously change its unconstrained shape due to one of six possible *local inelastic transformations* (LITs). The LITs were chosen to be of the pure shear type (no permanent volume change is allowed except for a transitory change related to the on-barrier configurations) corresponding to three elongations and three contractions along the symmetry axes of the hexagons (figure 1). Therefore, all six LITs are geometrically equivalent, except for their signs and orientations with respect to the symmetry axes.

The probability w per unit time for an LIT to happen is calculated according to the transition state theory of activated processes [12] as

$$w = \omega_0 \exp\left[-\Delta G^*(\sigma_{ij})/kT\right] \tag{1}$$

where ΔG^* is a stress-dependent free-energy barrier for an inelastic rearrangement that needs to be overcome, k is Boltzmann's constant, T is the absolute temperature and ω_0 is the frequency factor, related to a normal mode of structural fluctuation along the activation path.

The macroscopic response of the model solid is considered here as a net result of the individual LITs, and may be modeled if an appropriate Markovian stochastic process is defined. To randomly choose representative stochastic sequences of LITs a variant of the dynamic Monte Carlo (MC) method [13] was adopted, which is discussed in detail in I. Throughout the simulations a hexagonal mesh containing about 10 000 elements was used, therefore the total number of possible transitions for each current state of the model solid was about 60 000 with probabilities for each one of them calculated using (1).

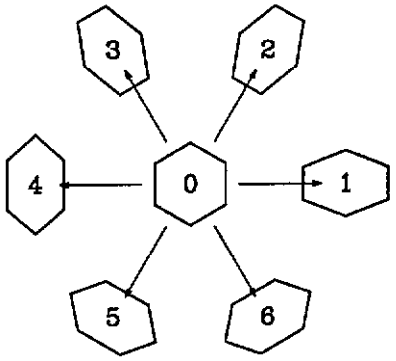

Figure 1. The complete set of six possible inelastic transformations.

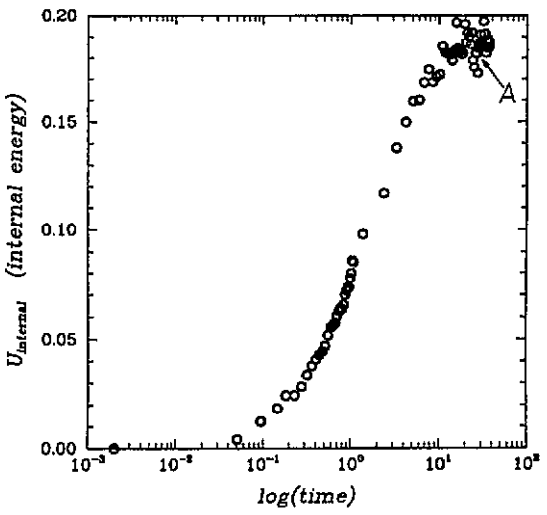

Figure 2. Kinetics of equilibration at $kT = 0.7$.

It is important to note, however, that in order to obtain a non-trivial numerical model we have explicitly accounted for misfit stresses due to reaction of the elastic surroundings to individual LIT's occurring in the system. Such interaction stresses, induced by the plastic transformations, were updated in all 10 000 'lattice' elements after each successful LIT. This was done using a pre-tabulated lattice Green tensor [14], which, by itself, reduced dramatically the number of computations performed at each step of the stochastic process.

Along with conventional periodic continuation conditions another type of boundary condition was also used, the 'dead matrix with buffer zone' model described in I. Coordinates, types and time intervals between subsequent LITs were recorded during simulations. Later these primary data were processed in order to obtain various characteristics of inelastic response, i.e., internal energy, spatial correlation functions and others. The developed code was flexible enough to allow the study of equilibrium as well as relaxation properties of the model solid under arbitrarily changing temperature conditions.

In I we introduced model parameters required to fully specify a model system. It was convenient to present all output in non-dimensional, reduced units in which the frequency factor ω_0, the area of the hexagonal elements Ω, the shear modulus μ and the inelastic shear strain increments e_s^* were all set equal to unity (in units of the fundamental scaling parameters that were introduced there). Remaining material constants were: zero-stress free-energy barrier for LITs $\Delta F_0^* = 0.785$ (in reduced units), dilatation in the transition state $e_d^* = 0.466$ (in reduced units), and Poisson's ratio $\nu = 0.25$.

As an example of the model at work we will discuss in this section equilibrium properties of the model system with the same material parameters as defined above.

Before proceeding with our discussions, however, it is useful to note that equilibrium properties of the model are not expected to depend on pressure at all, since completed LITs, defined to be of pure shear type, do not introduce any dilatation in the system and, thus, do not interact with pressure. Therefore, temperature is the only external parameter that affects the equilibrium properties of the model system. Furthermore, since material parameters ΔF_0 and e_d^* are related only to the transition states†, their choice affects only the kinetics and not equilibrium properties of the model.

This reasoning leads to the conclusion that in order to examine equilibrium properties of the model it is sufficient to obtain an equation of state in terms of, say, internal elastic energy as a function of the reduced temperature. To obtain a particular state of the system by the equation of state, the model solid was kept at some predefined temperature for a time interval long enough to allow the energy to reach its equilibrium level. One example of such equilibration is shown in figure 2 where the energy is plotted as a function of time for $kT = 0.7$. Initially all the elements were in untransformed states, and, therefore, the elastic misfit energy was zero. Then, after about 40 000 MC steps, the relaxing parameter reaches its equilibrium and remains unchanged, showing only fluctuations around the equilibrium level. Shown in figure 3 is a typical configuration of LITs, corresponding to the state marked A in figure 2. Different shades of gray show amplitudes of local transformation strain, the darker spots corresponding to the greater amplitudes of transformation shear strain. This picture shows that at such a high temperature ($kT = 0.7$) the equilibrium structure is characterized by a wide distribution of local shear misfit transformations showing no substantial correlations throughout the simulation cell.

Although it is possible to obtain the equation of state performing such thermalizations at different temperatures, the number of computations involved is quite substantial. Instead, simulations were performed of a relatively slow cooling rate ($q = -10^{-6}$) starting from some equilibrated state. The results are shown as circles (cooling) and squares (heating) in figure 4, while the corresponding evolution of internal structure is presented in figure 5.

The system energy decreases sharply in a narrow temperature interval around $kT \simeq 0.4$ resembling apparent discontinuity and hysteresis. The latter effect may be attributed in part to the finite size of the simulation cell, and in part to the finite rate of cooling and

† Although it seems logical not to assign any additional 'internal' energy and volume increment for the completed LITs, it is rather straightforward to introduce non-zero values if necessary.

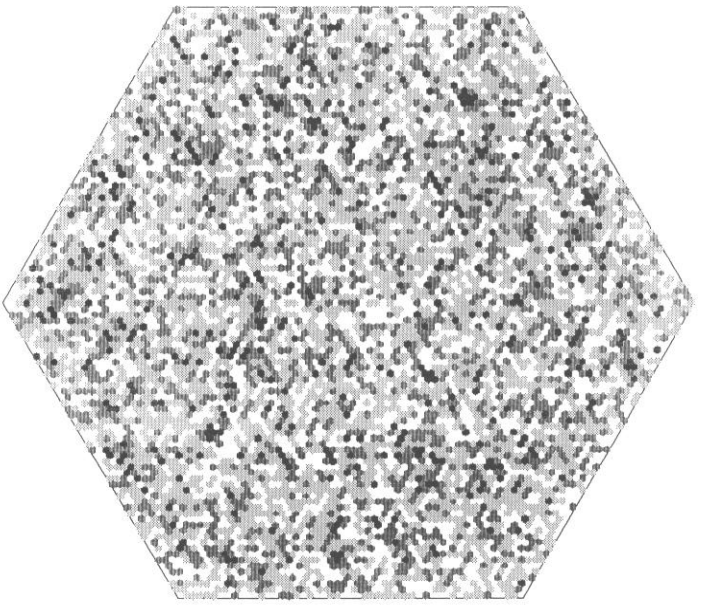

Figure 3. Configuration of LITS for the state marked A in figure 2.

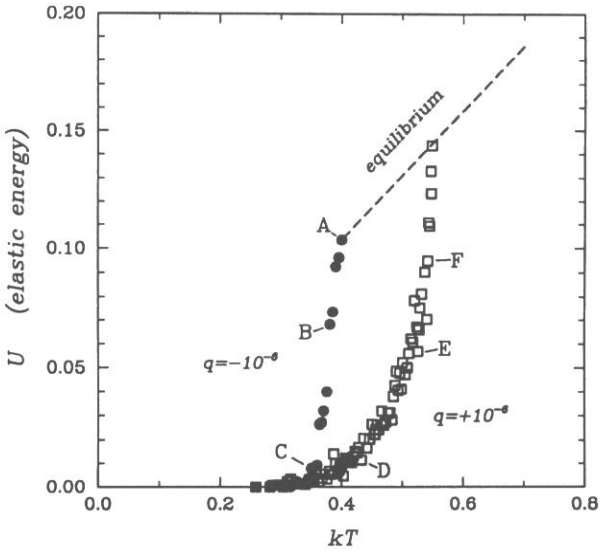

Figure 4. Elastic energy versus temperature—equation of state.

heating. The corresponding sequence of structures encountered during cooling is displayed in figure 5 (*a*)–(*c*). The observable increase in order is introduced through nucleation and growth of the ordered domains—i.e., crystallites. Indeed, although configuration A still shows substantial disorder, being apparently a state of subcooled melt, the system

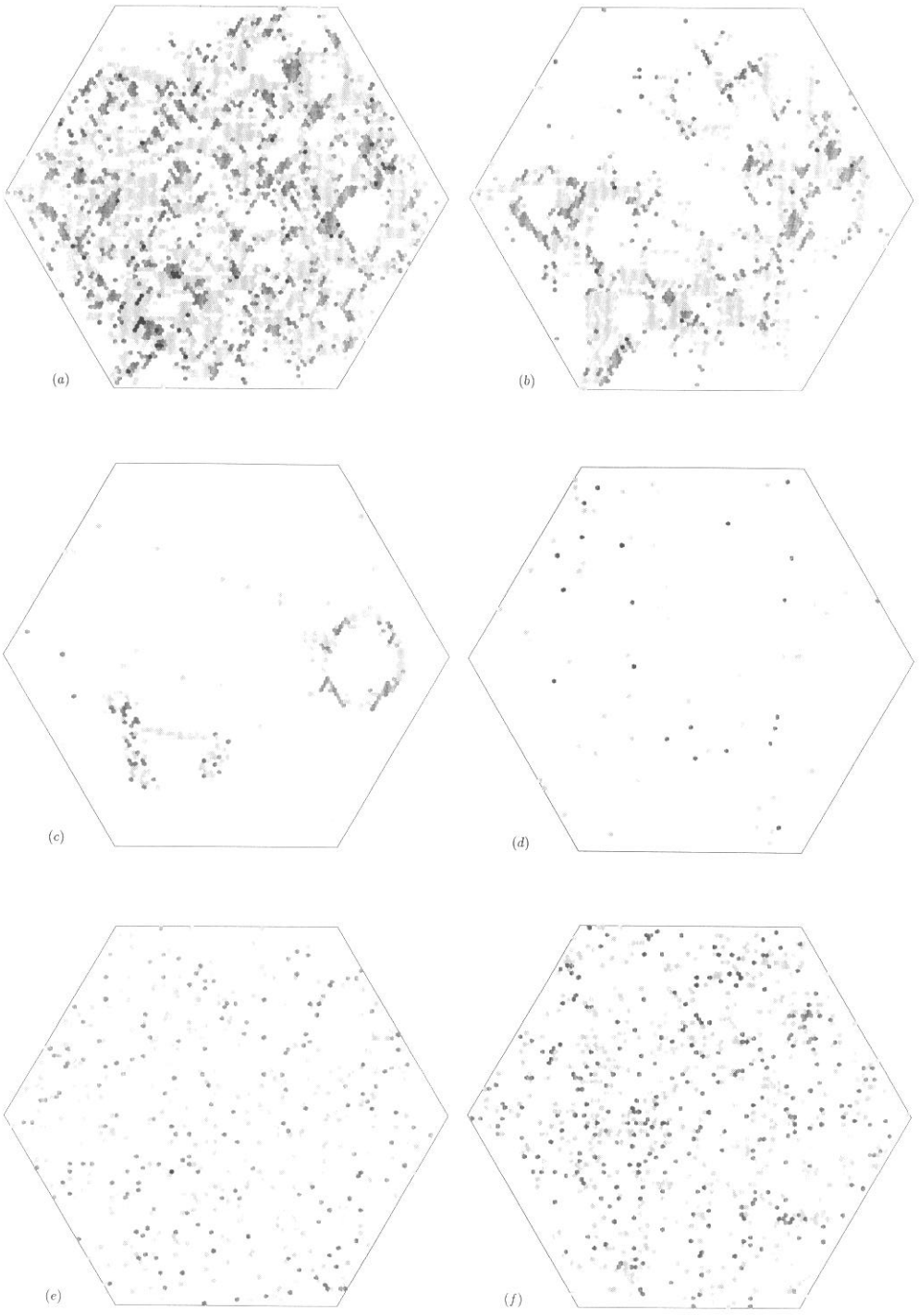

Figure 5. (*a*) Configuration of LITs for the state marked A in figure 4; (*b*) configuration of LITs for the state marked B in figure 4; (*c*) configuration of LITs for the state marked C in figure 4; (*d*) configuration of LITs for the state marked D in figure 4; (*e*) configuration of LITs for the state marked E in figure 4; (*f*) configuration of LITs for the state marked F in figure 4.

later becomes more ordered, while the remaining disordered domains separating crystallites systematically decrease in size (configuration B). Configuration C shows only very thin intercrystallite boundaries of rather unusual shapes. At later times these disappear as well. Parenthetically, ring-shaped disordered domains, one of which is clearly seen in figure 5(*c*), were always last to disappear in all the cooling simulations performed.

These observations indicated that the observed transition is of the first order, i.e., melting and solidification, which is in agreement with previous computer experiments on 2D atomic models [15, 16]. However, we note that there still exist different views in the literature on the order of the melting transition in 2D systems, since Kosterlitz and Thouless [17] and later Nelson and Halperin [18] and Young [19] have predicted continuous melting transitions with formation of intermediate hexatic phases. The controversy was partly resolved by Saito [20] who showed that in a 2D system of interacting dislocations the transition is of the first order if the dislocation core energy is small, but it is continuous for a system with a large core energy. Since dislocations may be viewed as particular combinations of LITs†, our model solid would appear to fall into the category of systems with a small dislocation core energy. This is not surprising since in the present model, the energy of any configuration is determined solely by the elastic energy of the corresponding misfit stress field. Nevertheless, if necessary, it should be possible to modify the model so that it may show a continuous order–disorder transition.

It is interesting to note that on heating the disorder was not introduced discontinuously, through nucleation and growth of disordered domains, but rather uniformly, showing no stable islands of disorder. It is not clear, at this stage, how such a *structural hysteresis* is to be interpreted. While the different behavior on heating and cooling may be related to the finite-size and finite-rate effects it should also be noted that the initial conditions are rather different. In any case, extensive simulations are needed in order to be able to reach more reliable conclusions on the thermodynamic and structural character of the observed transition.

3. Results and discussion

3.1. Vitrification. Kinetic phase diagram

As was mentioned in the previous section, equilibrium properties of model solids are fully characterized by a single equation of state if the properties involved are properly scaled. An appropriate scaling parameter for energy and temperature is the characteristic elastic shear energy of the distortion introduced by a single isolated LIT. This energy must scale as

$$E_0 = \mu e_s^{*2} \Omega \tag{2}$$

and has the dimensions J/m in the 2D model (and can be rescaled for a projection into 3D by dividing it by the layer thickness). However, such a universal scaling is not expected to apply to non-equilibrium states of a model since, even in the scaled form, there are still two other material parameters, ΔF_0 and e_d^*, which affect the kinetic properties of the model‡.

Below we address the following two questions.

† In his pioneering work Eshelby [21] demonstrated how dislocations and other discontinuous defects may be deduced as particular limiting cases of a more general formation—*the plastic inclusion.*

‡ We do not consider here the influence of Poisson's ratio ν on the observed effects simply because we have not performed any simulations with ν other than 0.25.

(i) Is it possible to obtain undercooled non-equilibrium states of the model system stable enough to be subjected to further deformation?

(ii) If the answer to (i) is yes, then how much is the relative glass-forming ability of a model system affected by a particular choice of the material constants?

First, the prominent hysteresis effect observed in the simulations of the equilibrium equation of state suggests that it is quite likely that undercooled states may indeed be obtained. However, prior to actually performing the simulations it is desirable to have at least a rough guide about which combination of the scaled material constants to choose in order to obtain undercooled states with a reasonable degree of success and acceptable expenditure of effort. The following simple reasoning helps to state essentials of the problem.

Consider the energetics of a single LIT occurring in an otherwise untransformed 'virgin' system. As was shown in I, the stress-free activation barrier for the first LIT to appear may be partitioned as follows:

$$\Delta F_0 = \Delta F^{\text{intrinsic}} + a(e_s^*)^2 + b(e_d^*)^2 \tag{3}$$

where $\Delta F^{\text{intrinsic}}$ is an internal free-energy barrier that is taken as an intrinsic property of the structure for the cooperative inelastic rearrangement as if it were to happen in the absence of the elastic surroundings, and the two last terms are the additional energy contributions representing the reaction of the elastic surrounding to the transformation occurring in the plastic core. Numerical factors a and b depend on the geometrical shape of the plastic core, and for a hexagonal element with unit area they are $a = 0.663, b = 0.326$. The second term on the right-hand side of equation (3) is related to the reaction of the elastic matrix to the shear component of a transitory shape increment, and, since e_s^* is set equal to unity, as a scaling choice, this term is simply equal to the geometrical factor a. The last term in equation (3) is due to the elastic resistance of the surrounding material to the dilatational component of the shape increment in the transition (on-barrier) state, and it is defined by the ratio of the transitory dilatation increment to the transitory shear increment, i.e., by the dilatancy ratio. It becomes clear now that all the parameters involved are related to the geometry and energetics of a particular mode of inelastic transformation, and that their magnitudes reflect, therefore, details of the interatomic interactions. These parameters may be estimated in principle from more detailed atomic-level simulations, and an example of how this can be done is given in the appendix.

In order to gauge how numerical values of the material parameters affect the kinetic properties of the model it is useful to consider, similarly to what was done in I, elastic energies for three particular states of the system. In these three states the energy is

(i) zero, for the initial virgin configuration,

(ii) $4a$, for a configuration with only one single element transformed, and

(iii) $\Delta F^{\text{intrinsic}} + a + b(e_d^*)^2$, for the intermediate transition state when the system is on the top of the potential barrier.

The potential barrier for the reverse transformation $1 \rightarrow 0$ is lower than that for the direct transformation $0 \rightarrow 1$, because of the misfit back-stress acting to restore the system to the initial stress free state 0. Actually, this barrier may be zero or even negative depending on particular values of the material constants $\Delta F^{\text{intrinsic}}$ and e_d^*. In such a case recovery will be immediate. Thus, a critical border-line condition may be defined as the case when the barrier for the reverse transformation is zero

$$\Delta F^{\text{reverse}} = \Delta F^{\text{intrinsic}} - 3a + b(e_d^*)^2 = 0. \tag{4}$$

Equation (4) is shown as the solid curve in figure 6, in the coordinates of two material parameters $\Delta F^{\text{intrinsic}}$ and e_d^*. This curve separates the region of expected instability towards spontaneous ordering ($\Delta F^{\text{reverse}} < 0$) and the region of systems expected to show some undercooling ability ($\Delta F^{\text{reverse}} > 0$). The barrier for reverse transformation becomes higher as $\Delta F^{\text{intrinsic}}$ and/or e_d^* increase, which is illustrated in figure 6, where the following condition $\Delta F^{\text{reverse}} = 1$ is shown as the dashed line. The origin of the coordinate axis corresponds to a system with a negative barrier $\Delta F^{\text{reverse}} = -3a$. The ability of systems to be stably undercooled is expected to grow as the state moves outward from the origin, and it is likely to be very low in the region below the solid curve. Alternatively stated, cooling rates required to obtain undercooled kinetically stable frozen-in configurations should become increasingly higher as the solid curve is approached from outside.

It should be noted, however, that the diagram given in figure 6 should only be considered qualitatively, since simulations have shown that even for a system with very low expected glass-forming ability ($\Delta F^{\text{intrinsic}} = 0$ and $e_d^* = 0$) rather stable ring-shaped clusters of LITs were observed if the applied cooling was fast enough. Nevertheless, the diagram even in its very simple form is quite useful in estimating relative glass-forming abilities of different systems before actually performing costly numerical simulations.

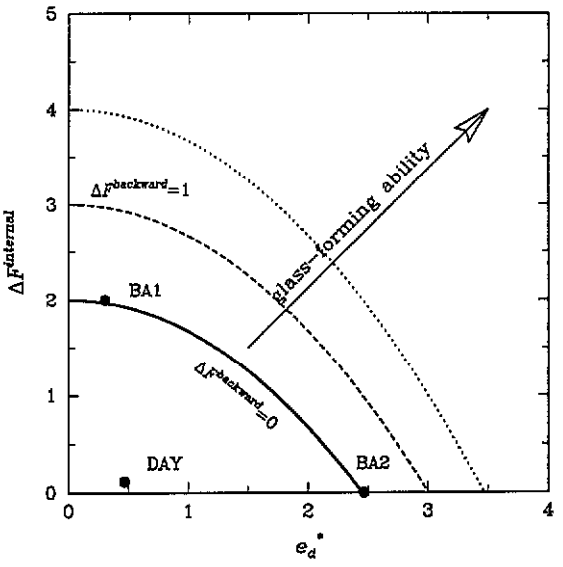

Figure 6. Kinetic phase diagram.

In order to show how such estimations can be performed, an example is given in the appendix for the 2D atomic model studied in [16]. The corresponding point marked as DAY in figure 6, which represents the conditions of that study, falls well inside the region of expected instability on the plane of the material constants. This agrees well with the observation made by the authors that it was virtually impossible to obtain frozen-in amorphous configurations for the single-component atomic model studied. It was shown in [16] that only at a rather high applied pressure did the system show a tendency to vitrify, which is also understandable in view of the fact that application of an external pressure p should increase the glass-forming ability of the system by decreasing relaxational mobility,

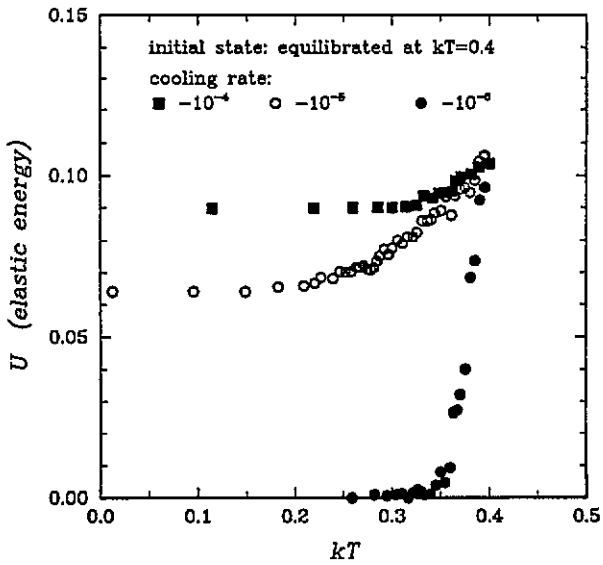

Figure 7. Simulations of cooling with different rates ('vitrification').

and corresponds to a shift of the approximate solid curve downward by a factor of the order of $e_d^* p$.

This example shows that a detailed analysis of inelastic transformations occurring in atomistic models, such as that given in [16], may provide the information needed to actually calculate the material constants for an equivalent continuum model discussed here. The latter can then be used for less detailed simulations of the very same systems, but for much larger sizes and for much longer time intervals.

The values of material parameters used in I and earlier in the present study were obtained based on the consideration of the above-mentioned atomic system. However, in order to obtain a more stable frozen-in structure another system was chosen with a higher intrinsic free-energy barrier

$$\Delta F^{\text{intrinsic}} = 2.0 \qquad e_d^* = 0.3 \tag{5}$$

so that the corresponding point on the diagram now moves directly on the solid curve (point BA1 in figure 6). This model system was cooled down from a well equilibrated high-temperature configuration at three different cooling rates: 10^{-4}, 10^{-5} and 10^{-6} (in reduced units). The system energy as a function of temperature obtained for all three cooling rates is shown in figure 7.

While at the lowest chosen cooling rate (10^{-6}) the energy of the system becomes zero soon after the temperature decreases below the transition point, at the higher cooling rates the system is no longer able to reach its equilibrium ordered structure in the time intervals available, and some disordered undercooled configurations are formed instead. These are shown in figure 8. The corresponding curves both show apparent changes in slope and non-zero residual energy, which is higher for the highest cooling rate (10^{-4}). It may be concluded, therefore, that the general appearance of the energy–temperature curves mimics an apparent glass transition, and the critical cooling rate for the system studied, with parameters given by equation (5), is in between 10^{-5} and 10^{-6}. Corresponding frozen-in

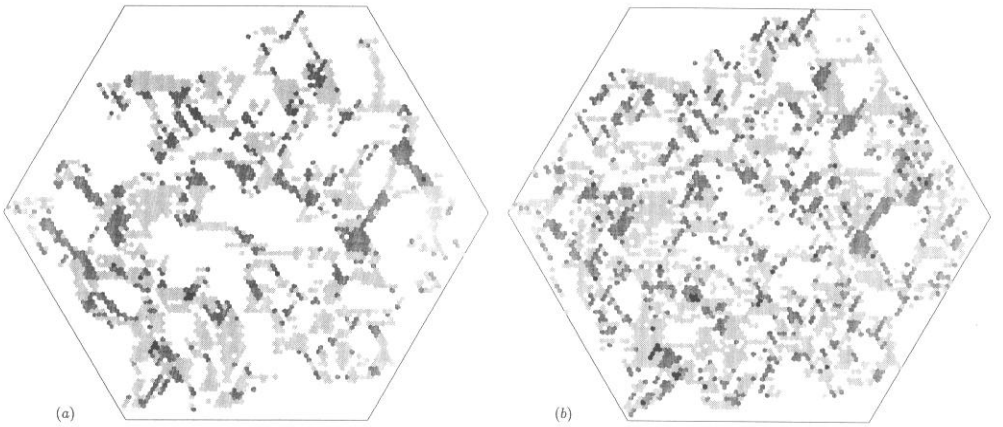

Figure 8. (*a*) Frozen-in configuration obtained after cooling with constant rate $q = 10^{-5}$; (*b*) Frozen-in configuration obtained after cooling with constant rate $q = 10^{-4}$.

structures show substantial disorder, which is higher for the configuration obtained at higher cooling rates, shown in figure 8(*b*), as can be gleaned by visual comparison with figure 8(*a*).

It is expected that the disordered structures obtained at such cooling rates will be kinetically stable on subsequent loading if it is conducted on the same or on a shorter time scale, i.e., with strain rates not lower than 10^{-5} (in dimensionless rate units).

3.2. Kinetics of structural relaxations

In this section our discussion will be focused on the following two questions.

(i) How much of the very complex kinetics of the structural relaxations can be depicted in the framework of the present simplified approach?

(ii) What is the influence of a particular choice of the material constants on the kinetics of simulated relaxations?

As was discussed earlier, the model shows certain attributes related to its ability to vitrify—such as hysteresis and apparent change in slope of energy versus temperature curves. However, real glasses have certain other common properties such as, e.g., non-linearity and asymmetry of isothermal structural relaxations, which are related to the fact that the relaxation kinetics depends not only on the thermodynamic conditions, i.e., temperature, pressure, etc, but also on current non-equilibrium states of the relaxing body [5]. In order to examine the capability of the model to describe such dependences, simulations were performed of isothermal relaxations of the model system with parameters chosen according to equation (5).

The results of two of such simulations are shown in figure 9. Initially configurations were obtained completely equilibrated at two different temperatures: $kT = 1.0$ and $kT = 0.4$. Then the temperature was suddenly changed and held constant† at $kT = 0.7$. It is quite

† For reasons that should become clear somewhat later, it was computationally very expensive to perform simulations of isothermal relaxations below the transition temperature. However, since we were only interested in the qualitative behavior of the model, most of the relaxation simulations were actually performed somewhat above the transition point.

clear that the high-temperature configuration responds to the sudden temperature change much faster than the low-temperature one, although both relaxations occurred at the same temperature.

It is interesting to note that both relaxation curves shown in figure 9 could be reasonably well fitted with a Williams and Watts (WW) [22]fractional exponent function

$$\Psi(t) = \frac{[U(t) - U(\infty)]}{[U(0) - U(\infty)]} = \exp(-t/\tau)^{\beta} \qquad 0 < \beta \leqslant 1 \tag{6}$$

where $\Psi(t)$ is the normalized relaxing property at time t, $U(0)$ and $U(\infty)$ are the actual value of the elastic energy at time t, at the beginning and at the end of relaxation, respectively, τ is a characteristic relaxation time, and β is the fractional exponent. It can be shown [5] that the fractional exponent β is inversely proportional to the slope of the WW function at its inflection point, and that the average relaxation time τ determines the position of the inflection point on the log(time) axis. The parameter β is also related to the width of the relaxation time spectrum, ranging from unity for simple exponential relaxations to zero for an infinitely broad relaxation spectrum.

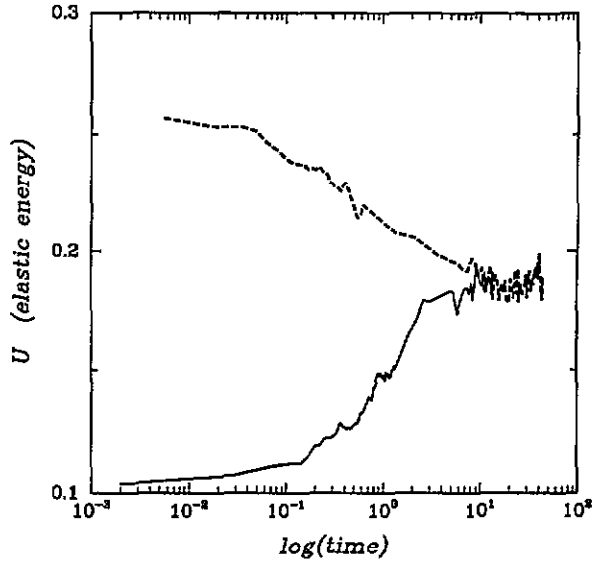

Figure 9. Kinetics of isothermal equilibration at $kT = 0.7$ after T jumps down from $kT_0 = 1.0$ (- - - -) and up from $kT_0 = 0.4$(——).

Best-fit values for the isothermal relaxations shown in figure 9 according to the WW expression were found to be $\tau = 0.3 \pm 0.1$ and $\beta = 0.92 \pm 0.06$ for the relaxation after the T jump from above (dashed curve in figure 9), and $\tau = 0.9 \pm 0.2$ and $\beta = 1.42 \pm 0.28$ for the relaxation after the T jump from below (solid curve). Even though these numerical values were obtained by averaging over three simulations for each relaxation regime there remained significant uncertainties as to whether, for example, the low-temperature relaxation showed meaningful deviations from the simple exponential kinetics.

Simulations showed, however, that the effects related to the distributed kinetics of relaxations were more pronounced for undercooled configurations at temperatures lower

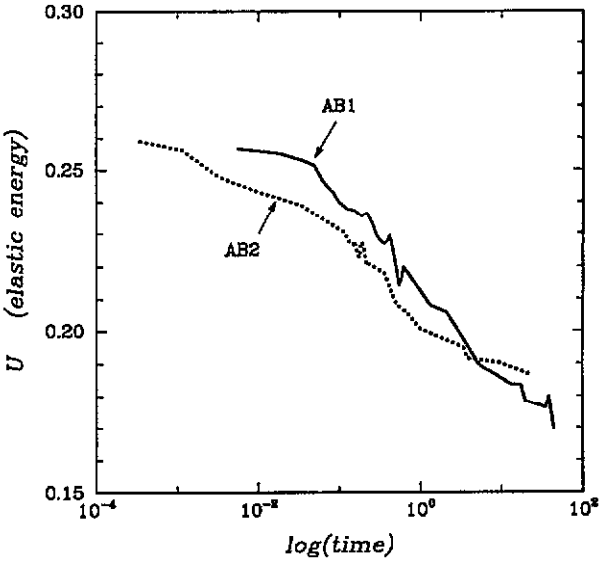

Figure 10. Kinetics of isothermal equilibration at $kT = 0.7$ after instant cooling down from $kT = 1.0$ for two systems with different values of parameter e_d^*.

than the transition point ($kT < 0.4$). Yet another way to make such effects stand out is to change the material parameters of the model. It is obvious, however, that a change in the intrinsic transition state energy $\Delta F^{\text{intrinsic}}$ may not affect the width of the observed relaxation-time distributions, since, according to equation (3), such a change corresponds simply to a uniform shift of time scales for all LITs, but the shape of the distribution is not expected to change. On the contrary, any change in the transitory dilatation increment e_d^* affects both the average relaxation time and the shape of the relaxation time distribution. For example, for a high value of e_d^* the distribution is expected to shift to longer times and to become broader as well.

Such an effect can be understood if we consider a typical equilibrium configuration at some temperature above the transition point. As was discussed earlier, such an equilibrium configuration is equally representative for all the model systems regardless of the particular values of the scaled material parameters $\Delta F^{\text{intrinsic}}$ and e_d^* chosen. However, the distribution of transition rates for LITs in the same configuration is broader for systems with higher values of e_d^*, since this parameter determines the sensitivity of the transition rates to the hydrostatic component of local misfits stresses. The same is probably true for non-equilibrium configurations that are, however, not so far from equilibrium.

To further examine the influence of the material parameters on the kinetics of structural relaxations, simulations were performed with a model system with zero intrinsic transition state energy $\Delta F^{\text{intrinsic}} = 0$, but with a rather high scaled transitory dilatation parameter $e_d^* = 2.45$ (point BA2 in figure 6). The idea behind such simulations was to compare the kinetic behavior of two systems, BA1 and BA2, both having the same total (intrinsic + elastic) transition state energy $\Delta F_0 = 2.63$ which was, however, composed in different ways.

It was expected that as systems BA1 and BA2 approach equilibrium at the same temperature the distribution of relaxation times should be broader for BA2 and narrower for BA1, but the overall time scale of relaxations would be about the same for both systems. Such behavior was indeed observed, as illustrated in figure 10 where the relaxing energy is

plotted against the logarithm of time elapsed after an instant quench down to $kT = 0.7$ of both systems BA1 and BA2 from the same equilibrium configuration obtained at $kT = 1.0$. The relaxation is steeper for BA1 than for BA2 or, from an alternative point of view, in BA2 relaxation starts earlier and ends later than in BA1 so that the two curves even intersect at some point. Averaged over three runs the values of best-fit WW parameters were found to be $\tau = 0.3 \pm 0.1$ and $\beta = 0.92 \pm 0.06$ for BA1 and $\tau = 0.26 \pm 0.14$ and $\beta = 0.78 \pm 0.09$ for BA2. Clearly, the value of the parameter β, as obtained for system BA2, is significantly less than unity.

It should be noted, however, that since the well known work of Kovacs [5] it is considered almost compulsory for a reasonable model of structural relaxations to be able to describe the so-called memory effects. In order to subject the model to such a test a configuration was obtained with a complex time–temperature history: first, system BA2 was instantly cooled down to $kT = 0.4$ from a well equilibrated state at $kT = 1.0$, then, after some time was allowed to undergo partial equilibration at $kT = 0.4$, the system was then suddenly heated up to $kT = 0.7$. The kinetics of the subsequent isothermal equilibration at $kT = 0.7$ is shown in figure 11 as the solid curve, where kinetics of plain relaxation after a single quench from $kT = 1.0$ down to $kT = 0.7$ is also shown for comparison (dashed curve). The configuration obtained after two subsequent T jumps shows rather complex behavior: the system energy first goes up and only then gradually decreases. Such relaxation kinetics is consistent with experimental observations and is related to the presence of both slow and fast relaxations in the system.

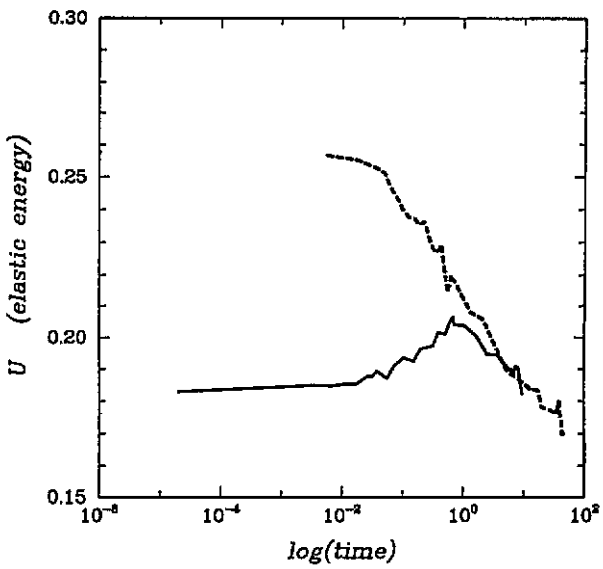

Figure 11. 'Memory' effect at $kT = 0.7$ (——) versus 'plain' equilibration (- - - -).

This and some other results discussed earlier show that it is possible to qualitatively describe certain characteristic features of relaxation kinetics in the framework of the present rather simplified approach, which was deliberately developed to ignore all but one factor, namely the influence of misfit stresses, contributing to the complexity of inelastic processes in solids. The good success of the present model in describing plastic deformation and structural relaxation properties demonstrates that the influence of the internal stress

distributions was not sufficiently appreciated in the past, even though the important role of this factor in the thermodynamics and kinetics of phase transformations in alloys has been clearly demonstrated by Khachaturyan and Chen [23,24].

This does not mean, however, that other factors are unimportant. Actually, a more relevant question that needs asking is, 'what are the relative contributions of the misfit stresses and other factors, such as anticipated intrinsic multimodality of inelastic processes, to the phenomena of interest?' The relative importance of the internal stress contribution is expected to vary substantially from one system to another since the major parameter, which to some extent determines the scales of variations of internal stresses, is the distortion energy $\mu\Omega(e_s^*)^2$ due to inelastic transformations. This is substantially different for, say, metallic and polymer glasses. Indeed, as could be estimated from the results of atomistic simulations reported in [10] (see also the appendix), this parameter for simple atomic glasses should be of the order of 10^{-18} J. At the same time for a typical polymer glass as studied in [9] the energy scale should be at least an order of magnitude smaller, due to the very small value of transformation strain parameter $e_s^* \simeq 0.02$ obtained for the studied polypropylene glass, although the transformation volume was found to be quite large, $\Omega \simeq 20000$ Å. It is expected, therefore, that the kinetics of structural relaxations in polymers is largely determined by the severe topological constraints to motions of polymer chains, and that the internal misfit stresses are relatively less important. In any case, whether misfit stress effects are dominant or only superimposed on some other more important effects it is essential to account for them in all amorphous solids. A relevant example may be given here of a long-debated problem in the literature of how to assign different regions of relaxation spectra to specific molecular motions in glasses of rather complex structure, such as amorphous polymers. As follows from the above discussion, peaks corresponding to otherwise distinct molecular motions may overlap or even become totally unresolved due to presence of the internal misfit stresses. This example shows that ignoring internal stress contributions may obscure the real physical picture of inelastic processes in disordered solids.

4. Conclusions

The results of numerical simulations, discussed in the present study, demonstrate the principal ability of the previously proposed numerical approach [1] to account for various experimental effects, related to ordering and disordering phenomena in solids.

In order to examine the equilibrium properties at zero-stress conditions, simulations were performed of cooling and subsequent heating of the model solid, which was previously well equilibrated at some high temperature and zero external stress. The internal energy versus temperature curve obtained in this way showed a phase transition of the first order which might be viewed as analogous to the crystallization–melting transition in real solids.

Furthermore, the kinetics of relaxations after sudden temperature changes were also studied as well as under conditions of continuously changing temperature. In spite of its simplicity, the model gives qualitatively correct descriptions of such well known phenomena as various hysteresis effects, stretched-exponential kinetics, non-linearity and asymmetry of isothermal relaxations, influence of cooling rate and hydrostatic pressure on the apparent T_g. Remarkably, even well known memory effects, usually considered as strong evidence for intrinsic multi-modality of the structural relaxations, were reproduced in the model which was based on a single type of LIT.

The structure of the model solid also showed a wide variability, ranging from highly disordered fast cooled configurations—'glasses'—to well aged configurations resembling

dislocation cells in crystals. In order to analyze the relative glass-forming ability of different model solids a kinetic phase diagram was used depending on two major scaling parameters of the model—the intrinsic transformation energy and the transient dilatation increment.

A practical result of the study of the structural relaxations was that it gave a means for obtaining and analyzing undercooled metastable structures with a controlled degree of frozen-in disorder, which was necessary for further studies of plasticity in disordered model solids [3].

Acknowledgments

This research was supported by a DARPA/URI program through the ONR under contract N00014-86-K-0768. Salary support for VVB was provided from a special fellowship from the William and Mary Greve Foundation and from an Allied Signal Corporation fellowship for which we are grateful to Drs John Kiser and Lance Davis, respectively.

Appendix

Here we give some details of calculations of parameters playing roles of material constants in the present model for a 2D single component atomic glass studied in [10]. In that study authors performed a molecular dynamics (MD) simulation of melting and quenching for a collection of 144 particles interacting via the Lennard-Jones pair potential function

$$\Phi(r_{ij}) = \epsilon_0[(r_0/r_{ij})^8 - 2(r_0/r_{ij})^4] \tag{A1}$$

where $\Phi(r_{ij})$ is the potential energy of interaction between atoms i and j at a separation distance r_{ij} and r_0 and ϵ_0 are length and energy parameters of the potential.

Initially all 144 atoms were arranged on a 12×12 grid in a hexagonal close-packed pattern (figure A1(a)). This 2D lattice was subjected to stepwise increases of temperature until the system melted. Then the melt was cooled by systematically reducing the temperature in order to obtain undercooled quasistable disordered structures.

Detailed analysis of the topology of the model in the above study showed that disorder was introduced upon melting usually in the form of two five- and two seven-sided Voronoi polygon quartets. Such structural defects are topologically equivalent to edge dislocations, which could be formed in a perfect lattice only in pairs. Once formed, such dislocations could move apart, annihilate or rearrange themselves on meeting with other dislocations. A possible topological representation of an event resulting in the spontaneous formation of two five- and seven-sided polygon dipoles (pair of two opposite edge dislocations) is shown in figure A1(b). Considering a small fragment of the close-packed structure containing only four particles, then the simplest possible rearrangement of atoms consists of moving two neighboring particles apart so that the other two may become closest neighbors. If initially a four-particle cluster is imbedded in the perfect lattice, then such a transformation corresponds exactly to the formation of a dislocation pair. In a less ordered structure such a correspondence is not so obvious, but still the discussed mechanism is expected to play a significant role there as well.

In any case, the assumption here is that the process shown in figure A1(b) is the only possible inelastic rearrangement solely responsible for the production of disorder and

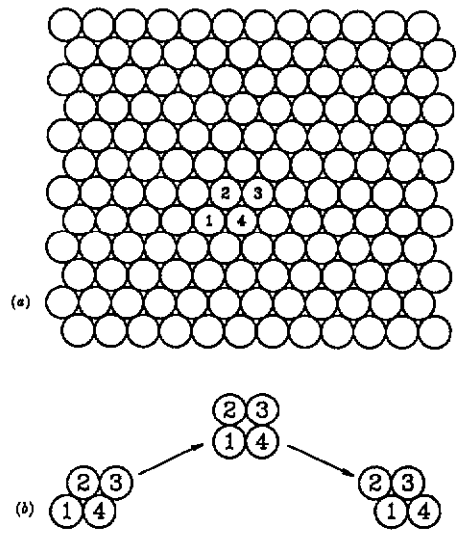

Figure A1. (*a*) Hexagonal close-packed structure; (*b*) Inelastic transformation of four-particle cluster.

ordering considered in the 2D atomic model. With this established, it becomes possible now to estimate geometrical and energetic parameters of LITs for the equivalent elasto-plastic continuum.

In order to find the transition-state energy $\Delta F^{\text{intrinsic}}$ for the rearrangement shown in figure A1(*b*) this event should be considered as happening in an isolated four-particle cluster. In such a case the initial untransformed configuration is that of two regular triangles with the edge length r_0 attached to each other through the common edge (here we neglect weak attractive interaction between particles 1 and 4). The final configuration also consists of two regular triangles, but arranged in a different way. Apparently the transformation is of pure shear type, without any dilatation produced.

From the symmetry considerations it is expected that the transitional on-barrier configuration should be a square (figure A1(*b*)), having some edge length r_1. This parameter was found from the condition of lowest energy of the square configuration of particles to be

$$r_1 = r_0(387/408)^{1/6}. \tag{A2}$$

Here we accounted for interactions of particles on diagonals of the square (1–4 and 2–3 in figure A1(*b*)).

Now it is possible to calculate the barrier by comparing the total energy of the four-particle cluster in transitional (square) and initial (rhombic) configurations. The result is that

$$\Delta\epsilon = U(\text{square}) - U(\text{rhombic}) = 0.519\epsilon_0. \tag{A3}$$

Using similar geometric considerations it is possible to also estimate the dilatation increment e_d^* and shear increment e_s^* in the transitional configuration as follows:

$$e_d^* = 0.135 \qquad e_s^* = 0.289. \tag{A4}$$

Our further assumption is that the shear modulus and Poisson's ratio for the equivalent isotropic elasto-plastic continuum may be estimated from the shear modulus and Poisson's ratio of the perfect hexagonal structure. The latter is anisotropic, however, the estimates needed are obtained as the angular averages. The values have been found to be

$$\overline{\mu} = 9\sqrt{3}\epsilon_0/r_0^2 \qquad \overline{\nu} = 0.25. \tag{A5}$$

Finally, written in the scaled form used through the present study, two major material constants for a continuous solid, representative of the atomic system studied in [10], are

$$\Delta F_{\text{intrinsic}} = \Delta\epsilon/\mu\Omega e_s^{*2} = 0.115 \qquad e_d^*/e_s^* = 0.135/0.289 = 0.466 \tag{A6}$$

where $\Omega = 2\sqrt{3}r_0^2$ is the area of the rhombic element.

These two numbers given in (A6) define the coordinates of the point marked DAY on the diagram in figure 6.

References

[1] Bulatov V V and Argon A S 1994 *Modelling Simul. Mater. Sci. Eng.* **2** 167
[2] Argon A S 1993 *Material Science and Technology* vol 6, ed R W Cahn, P Haasen and E J Kramer (Weinheim: VCH) p 461
[3] Bulatov V V and Argon A S 1994 *Modelling Simul. Mater. Sci. Eng.* **2** 203
[4] Turnbull D 1969 *Contemp. Phys.* **10** 473
[5] Kovacs A J 1964 *Fortschr. Hochpolym. Forsch.* **3** 394
[6] Kovacs A J, Aklonis J J, Hutchinson J M and Ramos A R 1979 *J. Polym. Sci.* **17** 1097
[7] Mazurin O V 1991 *J. Non-Cryst. Solids* **129** 259
[8] Chen H S and Turnbull D 1968 *J. Chem. Phys.* **48** 2560
[9] Mott P, Argon A S and Suter U W 1993 *Phil. Mag.* **67** 931
[10] Deng D, Argon A S and Yip S 1989 *Phil. Trans. R. Soc.* A **329** 613
[11] Johari G P 1984 *Relaxations in Complex Systems* ed K L Ngai and G B Wright (Arlington: Office of Naval Research) p 17
[12] Halsey G, White H J and Eyring H 1945 *Text. Res. J.* **15** 295
[13] Binder K 1986 *Monte Carlo Methods in Statistical Physics* ed K Binder (Berlin: Springer) p 30
[14] Teodosiu C 1983 *Elastic Models of Crystal Defects* (Berlin: Springer) p 260
[15] Allen M P, Frenkel D and Gignac W 1983 *J. Chem. Phys.* **78** 4206
[16] Deng D, Argon A S and Yip S 1989 *Phil. Trans. R. Soc.* A **329** 549
[17] Kosterlitz J M and Thouless D J 1973 *J. Phys. C: Solid State Phys.* **6** 1181
[18] Nelson D R and Halperin B I 1979 *Phys. Rev.* B **19** 2457
[19] Young A P 1979 *Phys. Rev.* B **18** 1855
[20] Saito Y 1982 *Phys. Rev. Lett.* **48** 1114
[21] Eshelby J D 1957 *Proc R. Soc.* **241** 376
[22] Williams G and Watts D C 1970 *Trans. Faraday Soc.* **66** 80
[23] Khachaturyan A G 1983 *Theory of Structural Transformations in Solids* (New York: Wiley)
[24] Chen L Q and Khachaturyan A G 1991 *Acta Metall. Mater.* **39** 2533
[25] Kohlrausch F 1863 *Pogg. Ann. Phys.* **119** 352

Modelling Simul. Mater. Sci. Eng. 2 (1994) 203–222. Printed in the UK

A stochastic model for continuum elasto-plastic behavior: III. Plasticity in ordered versus disordered solids

V V Bulatov† and A S Argon
Massachusetts Institute of Technology, Cambridge, MA 02139, USA

Received 26 January 1993, accepted for publication 3 August 1993

Abstract. The numerical approach, proposed by us in the accompanying papers, is applied here to simulate the plastic response of a 2D idealized elasto-plastic body under conditions of loading with constant strain rates. Various kinetic and structural aspects of plastic flow are extensively studied. The results of numerical simulations reproduce remarkably well various common features of plastic flow in solids, such as strain softening, strain rate and pressure and temperature dependences of plastic response at constant-strain-rate loading. Direct comparison of results obtained for model solids with different initial structural states shows that the character of plastic flow in transients is strongly affected by the degree of initial disorder.

1. Introduction

The character of the plastic response of different solids is known to depend on their packing structure and morphology, as well as on loading conditions. Since these may vary significantly it is not surprising that a wide variety of different mechanisms of plasticity has been considered [3]. In spite of such a wide variety of mechanisms, however, there are some aspects of plastic flow that are qualitatively the same for different solids, regardless of their chemical composition and packing structure. Among these are such effects as strain-rate and temperature dependences of plastic flow, influence of hydrostatic pressure and thermo-mechanical history, e.g. quenching or aging conditions, on the plastic properties of solids. Of course, quantitative details of plastic flow in different solids may differ significantly, but, at the same time, general trends, if we consider the influence of some particular factor on plastic behavior, are quite often the same for different solids. Along with the above-mentioned similarities in phenomenological features of plasticity there exist certain common structural alterations, accompanying plastic flow, such as localized plastic flow that can occur under certain conditions through nucleation and growth of shear bands [4].

In the present paper we continue with the development of the numerical model that was introduced in the preceding communication of this series [1], and further developed in [2] (hereafter referred to as I [1] and II [2], respectively). In this model both the processes of ordering and disordering and plastic flow in solids were treated on a common basis. The approach used was that both macroscopic plasticity and structural relaxations, responsible for the glass transition, are two net results of local inelastic transformations (LITs) occurring in small volume elements that can be interpreted as involving a few atoms or molecular groups. This approach deliberately ignored all but one factor, namely the influence of

† On leave from the Institute of Chemical Physics, Russian Academy of Sciences, Moscow, Russia.

0965-0393/94/020203+20$19.50

internal misfit stresses, contributing to the complexity of inelastic processes in solids. It was not intended to mean, however, that other factors are less important, nor did we question the very presence of internal misfit stresses in the solid body.

The question that was addressed in the preceding communications I and II was how much of the very complex picture of inelastic processes in solids might be attributed to the internal stress distributions present in the solid body.

The most important target of the present study is to further examine the capabilities of the proposed approach to account for various common features of plastic flow in solids and, more specifically, to compare the kinetics of the simulated plasticity in ordered and disordered solids† under similar loading conditions. Along with phenomenological characteristics of plasticity in crystals and glasses, the corresponding structural alterations that accompany plastic flow in our model are discussed.

It should be mentioned, however, that the numerical model in its present, rather simplified form may not provide a comprehensive quantitative analysis of the problem stated above. Nevertheless, as is shown below, the model is still very successful in describing various qualitative features of solid-state plasticity. This indicates that the important role of internal misfit stresses in the processes of interest was not appreciated enough in the past and deserves a much closer examination in the future.

In the next section the numerical approach, used here to simulate plastic flow under constant-strain-rate loading conditions, is specified, and a few necessary technical details are discussed.

Results of constant-strain-rate simulations in initially ordered solids are given in section 3 and section 4 contains a comparative analysis of plasticity in ordered versus disordered model solids. Results of the numerical simulations are summarized in section 5.

2. Details of simulations

The model discussed in detail in I and II is based on the assumption that plastic flow in a solid can be represented as a net result of local inelastic rearrangement of atoms or molecular groups. In order to numerically simulate such a process a 2D homogeneous isotropic linear elastic body is considered, which is arbitrarily tessellated into a regular hexagonal mesh. It is assumed, also, that each hexagonal element is able to spontaneously change its unconstrained shape due to one of six possible LITs, corresponding to three elongations and three contractions along the symmetry axes of the hexagons. It is not intended to associate any volume change with the LITs except for a transitory dilatancy allowed for the on-barrier configurations. Therefore, in order to keep the unconstrained volume (area) constant, compensating changes in transverse directions are assumed. For instance, for LITs numbers 1 and 4 eigenstrain tensors [5] are given as

$$\Delta e^{\mathrm{T}}_{ij}(1) = 2e^{*}_{\mathrm{s}} \begin{pmatrix} 1 & 0 \\ 0 & -1 \end{pmatrix} \qquad \Delta e^{\mathrm{T}}_{ij}(4) = -\Delta e^{\mathrm{T}}_{ij}(1), \ldots \tag{1}$$

where e^{*}_{s} is the amplitude of shear strain increments associated with the on-barrier activated configurations, and it is assumed to be exactly half of the shear increment $2e^{*}_{\mathrm{s}}$ for the fully developed LITs.

† Although the terms 'crystal' and 'glass' are occasionally used in the text, these, as well as the terms 'ordered solid' and 'disordered solid', are used only in the limited sense referring to the transformation-free and highly transformed random configurations of the 2D continuum solid, respectively, as discussed in II.

It is assumed that the LITs are produced by the combined influence of applied stresses and thermal agitations. Thus, the probability w per unit time for an LIT to happen is calculated according to the transition-state theory of activated processes [6] as follows:

$$\omega = \omega_0 \exp[\Delta G^*(\sigma)/kT] \tag{2}$$

where ΔG^* is a stress-dependent free-energy barrier for an inelastic rearrangement that needs to be overcome, k is Boltzmann's constant, T is the absolute temperature and ω_0 is the pre-exponential frequency factor.

The inelastic response of a model solid is simulated here by an appropriate Markovian stochastic process [7], and, in order to generate stochastic sequences of LITs, a variant of the dynamic Monte Carlo method [8] is adopted, which is discussed in detail in I.

The basic idea of such simulations is to account for internal misfit stresses produced by the plastic transformations occurring in the system. There are a few attempts reported in the literature to account for such stresses based on the approximate 'mean-field' arguments (see, e.g., [9]). In some instances, however, approaches of such a kind failed to provide an adequate description of the processes of interest, which is due to the fact that detailed spatial distribution of internal stresses was largely ignored there. Instead, in order to obtain a non-trivial numerical model, these stresses are explicitly accounted for here. Such interaction stresses need to be updated in all hexagonal elements after each successful LIT, and, for a mesh of any substantial size, this can be a formidable task if a finite-element approach is used. However, such updates were performed using a pre-tabulated 'lattice'† Green tensor [10], which, by itself, reduced dramatically the number of computations performed at each step of the stochastic process, and made it possible to simulate the plastic response of a hexagonal simulation cell containing about 10000 hexagonal elements‡ at reasonable expenditures of computer time.

Most of the simulations were performed using boundary conditions introduced in I that were specially designed to avoid physically unsound periodicity imposed on a system whenever the conventional periodic boundary conditions [11] are used. In this model the average stress was kept at some predefined level only in the central part of the simulation cell, as is described in detail in I and II. In the present study, however, modified boundary conditions were used allowing for control of the total (plastic + elastic) strain, rather than average stress, in the central 'core' zone. This was done to allow for simulations of plastic response under both 'constant-strain', and 'constant-strain-rate' loading conditions.

Initial frozen-in configurations, necessary for simulations of plastic flow in disordered solids, were obtained using the methods developed in II. Combining different cooling regimes with subsequent annealing at temperatures well below the order–disorder transition it was possible to prepare disordered undercooled configurations—glasses§—stable enough to allow for studying their plastic responses in a wide range of strain rates (typically 3–4 orders of magnitude of strain rates).

It is convenient to express all the model parameters (material constants and external control parameters), as well as all outputs of the simulations, in non-dimensional reduced units, introduced in I. Expressed in units of the fundamental scaling parameters, the

† The term 'lattice' is related here to the symmetry properties of the hexagonal tessellation and is not intended to imply that a crystalline state is necessary for the applicability of the model.

‡ The total number of possible transitions for each current state of the model was about 60000, with the probabilities for each one of them calculated using (2).

§ As was discussed in II, caution should be exercised in interpreting such configurations as representing real glasses. Nevertheless, we refer to them simply as glasses, having in mind that these structures are disordered and relatively stable.

frequency factor ω_0, the area Ω of the hexagonal elements, the shear modulus μ and the plastic shear-strain increment e_s^* on the activation barrier are all equal to unity. There remain only three material constants that specify completely the inelastic properties of a model solid†, and they were chosen to be for the present study

$\Delta F^{\text{intrinsic}} = 2.0$ – internal free energy activation barrier for LITs,
$e_d^* = 0.3$ – dilatation increment on activation barrier and
$\nu = 0.25$ – Poisson's ratio.

The kinetics of plastic flow was analyzed in terms of the average stress and the energy of internal stress distributions calculated and plotted as functions of the total strain. Structural alterations, accompanying plastic flow, were observed using methods of graphical representation introduced in I.

3. Constant-strain-rate deformation. Results for the ordered model solid

Results of numerical simulations of plastic flow in the initially ordered model solid under constant-strain-rate conditions of deformation are discussed in this section. Both kinetic and structural aspects of plasticity are considered for different regimes of shearing, including strain-rate, pressure and temperature effects.

It should be mentioned, however, that in the present model, as formulated in I and II, it is not possible to directly control total strain in the simulation volume. Instead, there are two other external control parameters—temperature and average stress—that may be changed arbitrarily. Nevertheless, it is still possible to perform the necessary simulations by adjusting the external stress applied to the simulation cell after each consecutive time increment, so as to maintain the total strain in the simulation volume (plastic + elastic) at a desirable level.

3.1. Low-strain-rate shear. Strain softening and accompanying structural variations

A $\sigma - \epsilon$ curve obtained in the simulation performed at a low temperature $kT = 0.15$ (well below the transition point) with a constant strain rate $\dot{\epsilon} = 10^{-5}$ is shown in figure 1. The loading was of pure shear type, with an extension along the 1 axis ($\epsilon_{11} > 0$) and the compensating contraction along the 2 axis ($\epsilon_{22} < 0$), so that the overall area of the simulation plane was kept constant. Below we consider in detail several subsequent states of deformed model solid, marked as A, B, C, D and E on the curve.

In the interval OA of strain the model solid deforms nearly elastically, with only few LITs produced, which, however, recover back almost immediately. A typical configuration of the simulation cell at this stage of deformation process contains at most one LIT, or no LITs at all. This indicates that the external stress exerted on the system to produce the required strain is not high enough to balance the back stresses acting to restore the initial untransformed state of the system.

Later, as the strain increases, the stress increases as well. LITs are produced at a higher rate and begin to form clusters (figure 2(*b*))‡. These small clusters form the nuclei of shear

† Physical meanings of the non-reducible material constants are discussed in detail in II.

‡ Darker shades of gray on the picture correspond to higher amplitudes of local plastic strain, and untransformed elements are shown as white.

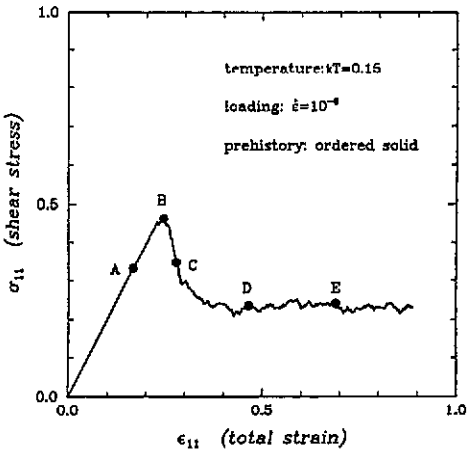

Figure 1. Stress–strain curve obtained for the initially ordered system loaded with constant strain rate $\dot{\epsilon} = 10^{-5}$.

bands†, that grow later at a high rate due to the combined influence of applied external stress and the stress concentration at the edges of shear bands (figure 2(*c*)). It becomes possible now to maintain the required strain rate at a lower level of external stress, which decreases rapidly after reaching its peak level. This effect is due to very high internal stresses exerted on the elements near the edges of the already developed shear bands, as explained below. Eventually, some steady-state level of stress is established, corresponding to dynamic equilibrium of the flow structure with the applied strain rate (interval B–C–D in figure 1).

In the case discussed here two major mechanisms of plastic strain production can be clearly distinguished: the nucleation of new shear bands (i), and the propagation of the shear bands by incorporating in them more and more elements (ii). It is likely that the nucleation of new shear bands is more probable at higher levels of shear stress, while at lower shear stress the mechanism of propagation of shear bands dominates at otherwise equivalent loading conditions. The reason for this becomes clearer if we consider how many elements can be active in producing additional plasticity at different levels of shear stress. It is clear that the higher the stress the greater the fraction of elements that may undergo LITs in time intervals characteristic for a given strain rate. However, the fraction of plastically active elements may decrease substantially whenever the external stress decreases for some reason. In such a case only those elements that have significantly higher than average levels of internal negative pressure and/or internal shear stress, superimposed with external shear stress, may effectively participate in the production of plastic strain on the time scale of the applied loading regime, but then only until the favored elements are exhausted. An interesting result of such behavior may be seen in the interval B–C–D, where all isolated LITs and the smallest of shear bands, formed at the peak level of shear stress (figure 2(*c*)), return back to the untransformed state (figure 2(*d*) and (*e*)) so that only three major shear bands survive. It is clear that a rather high level of shear stress is necessary to create the ingredients of a flow structure, which develops after certain evolutions into the three

† The term 'shear band' is used here in its most generic sense, related to any formation of quasi-linear shape containing shared material. Under such a definition any dipole of edge dislocations, formed in the 2D system and moved some distance apart, may be viewed as an example of a very thin shear band. A few such 'shear bands' are present in figure 3(*c*).

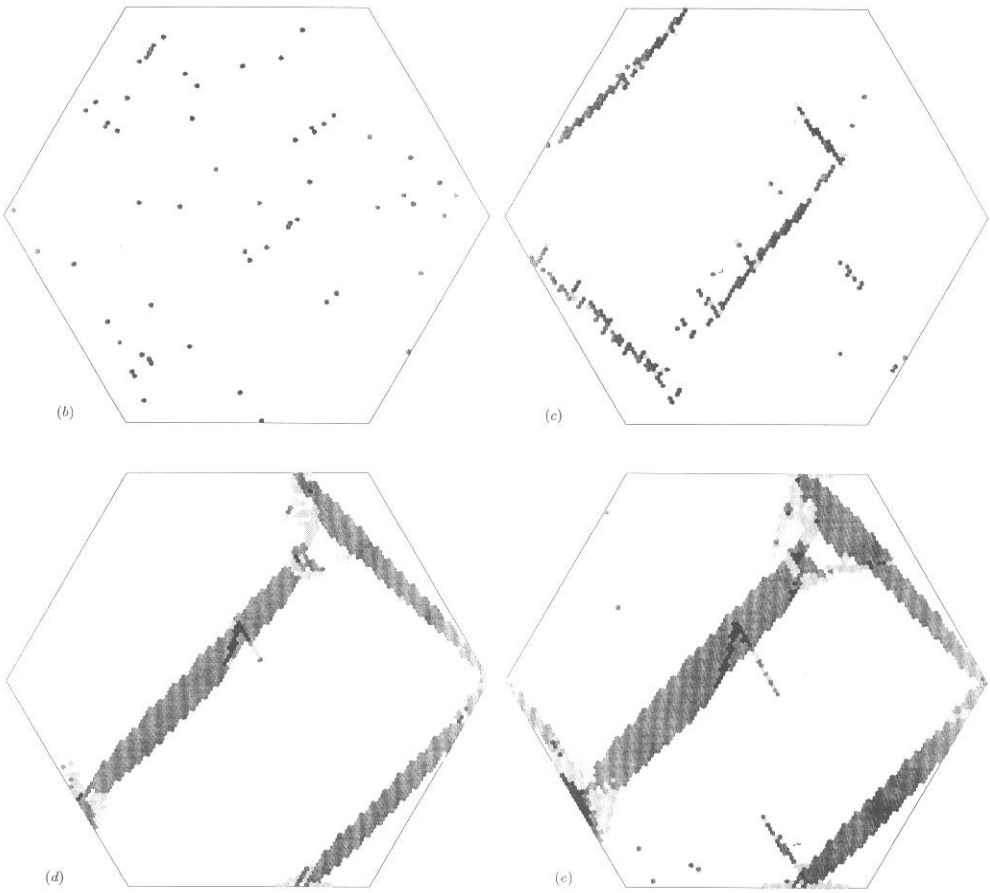

Figure 2. (*b*) Flow structure for the state marked B in figure 1; (*c*) flow structure for the state marked C in figure 1; (*d*) flow structure for the state marked D in figure 1; (*e*) flow structure for the state marked E in figure 1. (Note figure 2(*a*) is not of significance and is therefore omitted.)

major shear bands bearing the whole burden of plastic flow. At the same time as the stress decreases, some of the smaller shear bands become sub-critical in a sense that internal back stresses at their edges now exceed the level of externally applied stress. Therefore, the observed *upper yield hump* and the subsequent *strain softening* reflect particular stages of the development of *flow structure*. The resemblance of this behavior to initiation of plastic flow in some cases of crystal plasticity [12] is striking.

As was proposed in I, the process of plastic flow may be analyzed in association with the distribution of internal stresses. Several sequential stages of development of the internal stress distribution in the simulation cell are shown in figure 3. The distributions were calculated for the 11 component of the internal stress for the same five states of plastic deformation as discussed above and marked A, B, C, D and E in figures 1 and 2. Initially, in the interval OA of the quasi-elastic response, the internal stresses are very small since only isolated LITs occur at this stage of the deformation process (distribution A in figure 3). However, as the external shear stress reaches its peak level the distribution broadens and becomes skew (distribution B). On further straining both the width and the skewness continue to grow, and two other peaks are formed at the higher and lower ends

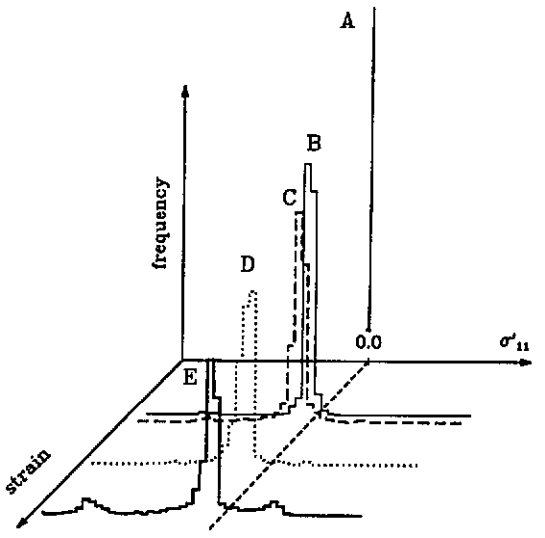

Figure 3. Evolution of the internal stress distribution function (11 component) calculated for the same loading simulation as figure 1.

of the distributions (distributions C, D and E). The formation of these peaks coincides with the onset of shear localization, and reflects increasingly high concentration of the internal stresses at the edges of the shear bands. Analysis of the internal stress distributions shows that, in a case when plastic flow is highly localized, all the elements in the simulation volume may be grouped into the following three distinct classes:

(i) elements at the edges of shear bands that were recently transformed and experience high back-shear stresses (corresponding to the lower end peak of the distributions);

(ii) elements near the edges of shear bands that experience high positive internal shear stresses superimposed on the external shear stress, and are expected to transform in the next few steps of the stochastic process (the higher end peak);

(iii) all other elements (the central part of the distribution), including the elements in the middle of shear bands where misfit stresses are not nearly as high as at and near the edges.

When shear localization is strong, only the elements from group (ii) are active in producing plastic flow†. On the other hand, new shear bands are initiated from the elements corresponding to the high-stress end of the third group.

Conditions of stable growth for a given shear band may be obtained on the basis of a consideration of the ratio of the probabilities of the relevant elementary processes, as was done in I and II. The process that contributes to shear band propagation is the production of LITs in the elements near the edges of the shear band that belong to class (ii). On the other hand, the shear band may shrink as a result of a reverse transformation in the elements at the edges of the shear band (class (i)). For a shear band to grow stably the probability of propagating should be higher than the probability of shrinking. It follows from the comparison of these two probabilities that the condition of criticality is stress dependent, and the critical length of shear bands that can just grow is smaller at a higher applied shear

† Plastic flow of such a kind is usually described as mobility controlled [13].

stress†. Thus, in view of the present analysis, the observed transient over-production of shear band nuclei (figure 2(*c*)) is considered to be quite realistic.

It should be noted here that the Gaussian form used in I of the internal stress distribution function is not accurate, and it may not be used for a quantitative characterization of the internal misfit stresses. In fact, in a case of strong shear localization the distribution of misfit stresses becomes prominently tri-modal, and the Gaussian approximation is totally inadequate in such a case. Nevertheless, analysis of plasticity in terms of the internal stresses is essential, regardless of the shape of the internal stress distribution that builds up in the system.

Another parameter that was introduced in II was the elastic energy of the internal misfit stresses, which characterizes the degree of structural inhomogeneity of the plastic strain distributions. The elastic energy of the misfit stresses‡, per element of the simulation volume, expressed in units of the fundamental scaling parameters, is shown in figure 4 as a function of the total strain for the same simulation as discussed above. In the interval of quasi-elastic response this parameter is nearly zero. Later, however, it shows a stepwise change in a narrow interval of total strain A–B–C. Such behavior reflects dramatic changes in the internal structure of the model solid that take place in the interval of the peak stress where the elements of the flow structure are established. Then, in the interval of stationary flow, the energy is nearly stationary also. The later increase (beyond point E) is an artefact of the boundary conditions used.

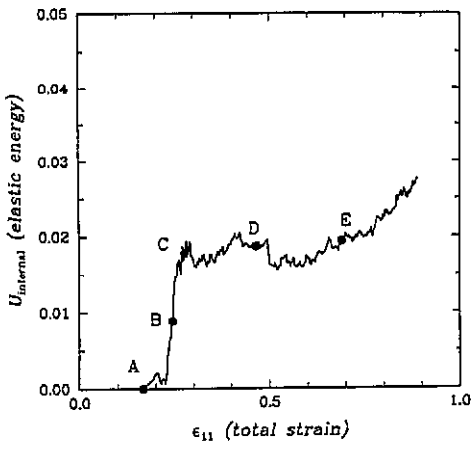

Figure 4. Energy of internal misfit stresses as a function of total strain calculated for the same loading simulation as in figure 1.

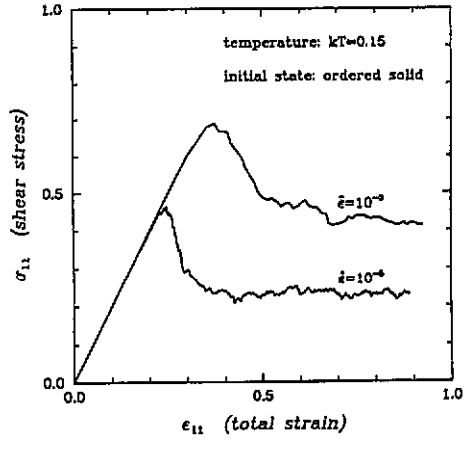

Figure 5. Stress–strain curves obtained for the initially ordered system loaded with different strain rates.

Concerning the artefacts of the model, it should be mentioned that both the periodic continuation and the 'dead-matrix' boundary conditions introduced in I and II have their disadvantages. Thus, the above-mentioned increase of the internal elastic energy, observed

† This result is well known (see, e.g., [14]) in relation to critical cracks and the critical size of dislocation loops. For cracks it is customary to relate such effects to the stress intensity factor at a crack tip, which is known to grow as the square root of the crack length with increasing crack dimensions. For dislocation loops (or dipoles) where a lattice resistance to shear may be present, the criticality condition is slightly more complex.

‡ Another contribution to the total elastic energy due to uniform external stress is not considered here.

only for the 'dead-matrix' model, is due to the fact that in this case the surrounding matrix is not allowed to accommodate to the very high local misfits (figure 2(*c*)) by propagating the shear beyond the boundaries. This leads to the inevitable build-up of the misfit stresses along the boundaries, and in the corners of the hexagonal simulation cell. This effect is more pronounced at higher strains. Simulations performed using the periodic boundary conditions are free of such undesirable effects, but, in turn, such simulations result in lower-than-expected values of the yield stress and steady-state flow stress. These artefacts are due to strong interactions of shear bands with their own periodic images, which is particularly important for the model discussed here, since the elastic interactions considered are of a long-range character. It is a good practice, therefore, in order to obtain more reliable results, to perform simulations using different boundary conditions at otherwise equivalent loading conditions and to examine the results.

3.2. Strain rate effect

Figure 5 shows two stress–strain curves obtained in simulations performed under conditions of constant-strain-rate loading with two different strain rates $\dot{\epsilon} = 10^{-5}$ (shown also in figure 1) and $\dot{\epsilon} = 10^{-3}$. The curve obtained at the higher strain rate shows substantially higher values of the peak stress at yield which, however, were reached in a much shorter time interval. The subsequent reduction of stress, i.e., the strain softening is only a little greater than that obtained at the lower strain rate, and the steady-state level of stress is, therefore, substantially higher. Comparison of the peak stresses and the steady-state stresses for the two temperature conditions here revealed that there is neither a proportional stress drop nor a constant strain softening when these two cases are compared. Rather, the real situation lies somewhere in between these two idealizations.

In the case of the higher-strain-rate loading, the observed higher peak stress is due to the necessity of creating a flow structure in a shorter time. As soon as shear bands are formed, the stress drops within a small increment of strain, since such a high level of stress is not needed to maintain the required strain rate once the necessary elements of strain production are present. However, the equilibrium, steady-state level of flow stress, established shortly after the yield point, is still considerably higher than that for the lower-strain-rate flow. Again, the analysis of the internal stresses helps to relate the observed kinetic behavior to the corresponding structural alterations.

As in the case discussed in the previous subsection, the overproduction of shear band nuclei is observed here as well. However, a large number of shear bands survive the stress drop in the case of the higher strain rate (compare figure 2(*d*) and figure 6). These shear bands are sufficient to maintain a higher plastic strain rate than in the previous example in the steady-state flow regime. Also, since the equilibrium stress is higher at the higher strain rate, the shear bands are notably smaller now, but still super-critical (figure 6).

The flow structures produced in the higher strain rate simulation are characterized by a higher degree of non-homogeneity, which is reflected in the higher level of misfit energy accumulated mostly in the transient interval, as can be seen in figure 7.

3.3. Hydrostatic-pressure effect

It is not necessary to perform any additional simulations in order to examine the effect of hydrostatic pressure on the kinetics and the structural features of plastic flow. Indeed, as can be shown based on (14) of paper I, an increase in the hydrostatic pressure by an amount Δp at a given temperature T produces a uniform decrease in the rates of all possible LITs by a factor of $\exp(-e_{\mathrm{d}}^{*}\Delta p/kT)$. Therefore, in the present model, an increase in the

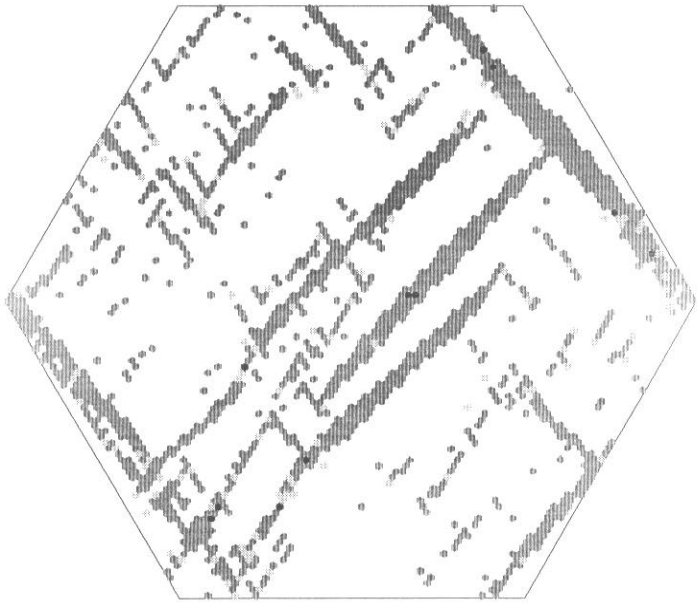

Figure 6. A flow structure obtained under conditions of loading with high strain rate $\dot{\epsilon} = 10^{-3}$.

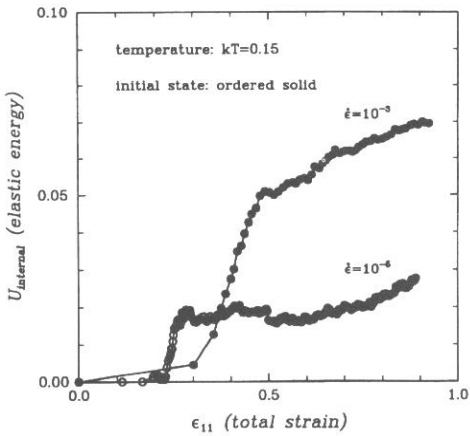

Figure 7. Energy of internal misfit stresses as a function of total strain for simulations performed at different strain rates.

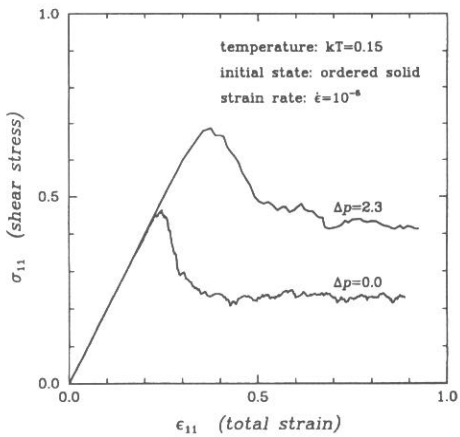

Figure 8. Stress–strain curves obtained in simulations performed under different pressures.

hydrostatic pressure produces the same effect as the corresponding increase in the strain rate. Alternatively, since for the studied model solid BA1 $e_d^* = 0.3$, the curve obtained at $kT = 0.15$ with the strain rate $\dot{\epsilon} = 10^{-3}$ may be equally interpreted as obtained at the lower strain rate $\dot{\epsilon} = 10^{-5}$, but under an additional hydrostatic pressure of

$$\Delta p = \log_e(100)kT/e_d^* = 2 \times 2.303 \times 0.15/0.3 \approx 2.3. \tag{3}$$

In order to illustrate the discussed equivalence figure 5 is plotted again, this time as

figure 8, but the curve obtained at the higher strain rate is interpreted now as being obtained at the high pressure. In view of this equivalence, all the discussion given in the previous subsection about the differences in the kinetic and structural aspects of flow at different strain rates is applicable here as well.

Another interesting question that is relevant to the present discussion is: 'How realistic is *the principle of the pressure–strain-rate superposition* that is accurate for the model considered here?' Although it is not expected that this rather idealized principle holds exactly in real situations, still, general trends observed in experiments [15, 16]† follow the pattern in many cases.

3.4. Temperature effect

To examine the influence of temperature on plastic flow in the initially ordered solid simulations were performed of deforming with the low strain rate $\dot{\epsilon} = 10^{-5}$ at a constant temperature $kT = 0.13$, which was a little lower than that in the previously discussed simulations ($kT = 0.15$). However, even such a small reduction of the temperature results in a prominent change of the peak stress at yield, which is almost three times higher for the lower-temperature simulation, as is shown in figure 9. The subsequent very sharp drop in stress observed in the simulation is related to a catastrophic development of events occurring on the structural level with the features of a threshold character. Figure 10 gives another view of the threshold-type behavior of initiation of plasticity at this low temperature, where the different rates of build-up of the energy density at the flow state are given for the two temperatures of $kT = 0.15$ and 0.13. Indeed, a detailed analysis of the simulation data showed that more than half of the plastic strain, accumulated to the end of the simulation, was actually produced almost instantly, i.e., in a very narrow interval of strain of about 10^{-4}.‡ In such a very short time interval the flow structure evolves dramatically, beginning from the nucleation of small elongated shear clusters (figure 11(*a*)), to the development of a single major shear band and a few smaller ones (figure 12(*b*) and (*c*)). Comparison with the structures obtained at the higher temperature $kT = 0.15$ (figure 2), shows that the total number of shear bands that survived the stress drop in the lower-temperature simulation is about the same as that observed in the higher-temperature case. This may be explained by recalling that the criticality condition for the initiation of stable shear bands depends primarily on stress, and very little on temperature, and that the flow stress that the systems settle down to after the yield drop is almost at the same level for both temperatures considered.

The fact that the level of stress at steady-state flow is only slightly higher (about 10%) in the lower-temperature simulation suggests that both temperatures that were considered are low enough for the propagation of shear bands to occur almost athermally. However, a slight increase in the equilibrium stress is still required at the lower temperature to compensate for less intensive thermal agitations.

Another interesting feature of the lower-temperature flow structure that needs to be explained is the observed dominant development of a single shear band after the steady-state regime is established. This effect is likely to result from the fact that at such a low

† It is not always possible even to make necessary comparisons with experiments, since there are not many data reported in the literature from which the influence of the pressure on plastic flow can be directly deduced. Also, in some cases the intervention of fracture makes it impossible to examine the relations discussed.

‡ Such near-threshold-like behavior in initiation of plastic flow is characteristic of the response near absolute zero temperature, where in the absence of thermal motion plasticity is initiated at a higher stress at an arbitrary high rate [12].

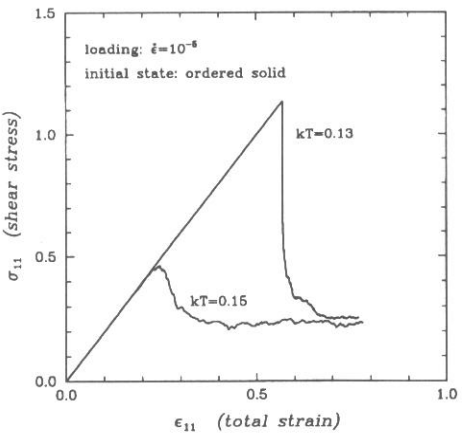

Figure 9. Stress–strain curves obtained for the initially ordered system loaded with the same strain rate ($\dot{\epsilon} = 10^{-5}$) but at two different temperatures.

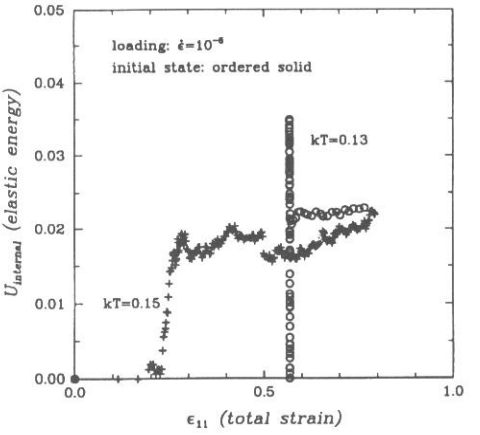

Figure 10. Energy of internal misfit stresses as a function of total strain obtained in the same simulations as the curves in figure 9.

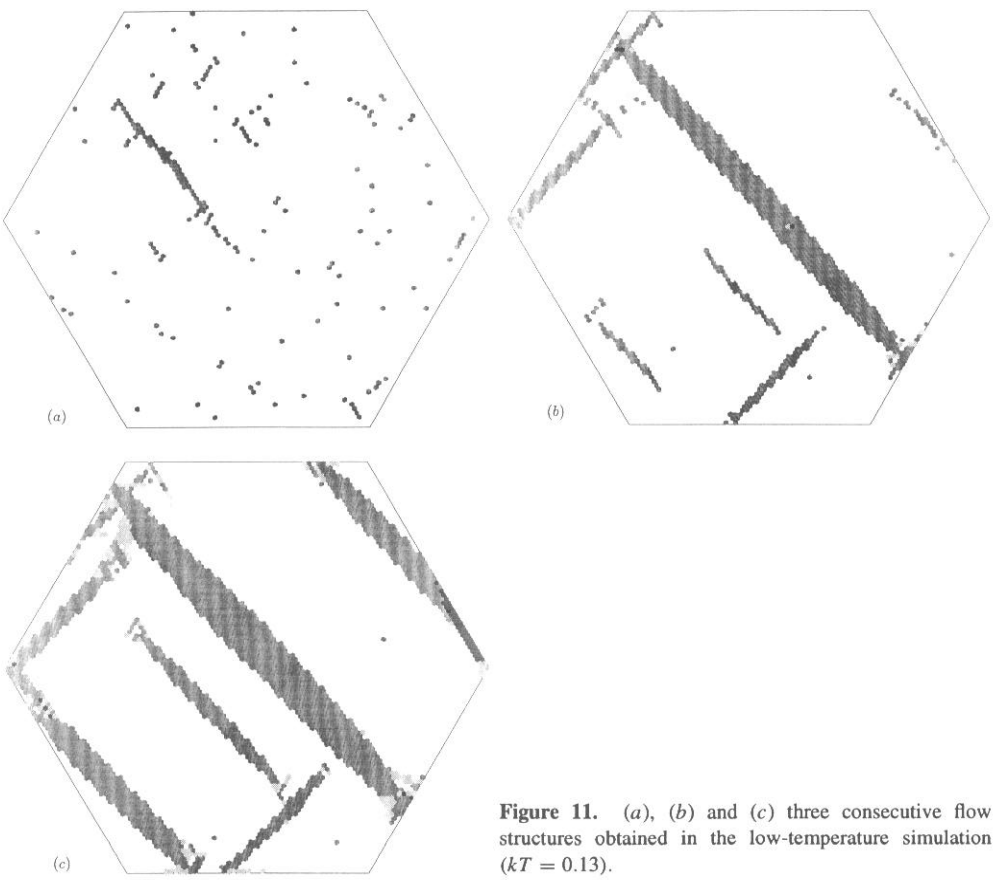

Figure 11. (*a*), (*b*) and (*c*) three consecutive flow structures obtained in the low-temperature simulation ($kT = 0.13$).

temperature, when thermal agitations do not contribute much to the observed plastic strain

rate, one of the shear bands with the largest aspect ratio that survived the stress drop grows notably faster (no doubt due to the higher stress concentrations that it sets up) than others, even though they all are super-critical at such a level of stress. This effect is expected to become increasingly more pronounced at lower temperatures as is observed.

4. Deformation of disordered solids

4.1. Influence of thermo-mechanical history on the stress–strain curves

It was the objective of one of the preceding contributions (II) to develop methods of obtaining undercooled structures with a controlled degree of disorder. First, the model elasto-plastic body was cooled down at some cooling rate from a well equilibrated configuration obtained at a temperature well above the order–disorder transition. Then undercooled configurations obtained in this manner were aged at low temperatures for different time intervals in order to reduce frozen-in disorder to a desired level. Depending on the cooling rate and/or the conditions of subsequent aging, various structures with certain amounts of residual disorder were obtained that were stable on the time scale appropriate for further deformation simulations (typically 10^4–10^6 time units).

In this section two particular initial configurations are considered, referred to hereafter as *quenched glass* and *aged glass*, that were obtained by cooling an equilibrium random configuration of *melt* from $kT = 0.7$ down to $kT = 0.15$ at a constant cooling rate of $q = -10^{-5}$. The quenched glass corresponds to the disordered configuration that was obtained immediately after the cooling, while the configuration of the aged glass was obtained by subsequent aging of the quenched glass at $kT = 0.15$ during a time interval of 10^6 time units. These two configurations are characterized by different amounts of residual disorder, the aged glass being less disordered, as is expected.

Results of numerical simulations performed under conditions of deformation with a constant strain rate of $\dot{\epsilon} = 10^{-3}$ at $kT = 0.15$ for the two disordered solids are shown in figure 12 along with the stress–strain curve obtained for the initially ordered solid at the equivalent loading conditions (see also figure 5) shown for comparison. These simulations demonstrate clearly that the nature of the initiation of plastic flow is very sensitive to variations of initial structure of the model solid. Indeed, while the aged glass, being closer to an ordered solid, shows some strain softening, the quenched glass, with a higher degree of disorder, does not. Another interesting feature is related to the amount of strain softening observed, which is substantially higher for the ordered solid (crystal) than for the initial configuration of the aged glass. Again, we find it instructive to analyze these differences in terms of the internal misfit stresses.

In the case of the ordered solid, the initial perfectly ordered structure has to be destroyed first, and then an appropriate flow structure has to be created in order for the system to flow at a required rate. Since disorder has to be nucleated in the perfect solid, which resists structural alterations, a high stress is necessary to overcome this resistance to nucleation of flow units, and, therefore, a relatively high yield stress appears in this case, as was demonstrated previously in section 1.

Analysis of internal misfit stresses performed for the configuration of the quenched glass showed that the distribution of these stresses was centered around a single peak, located near zero internal stress, unlike the distribution of stresses for the plastically deformed solid, which was found to show three distinct maxima (see section 3.1). However, it is not the shape, but rather the width, of the internal stress distribution that is responsible for the observed lack of strain softening in this case. Indeed, the half-width of the distribution was

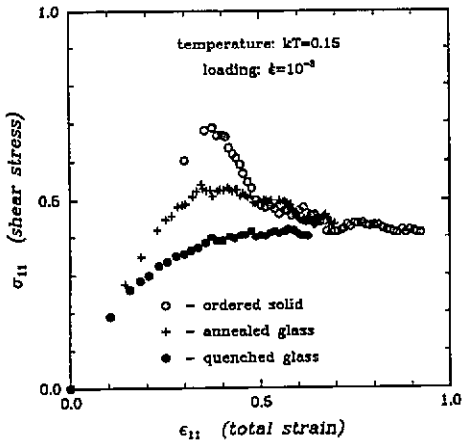

Figure 12. Stress–strain curves obtained in simulations under constant strain rate loading conditions ($\dot{\epsilon} = 10^{-3}$).

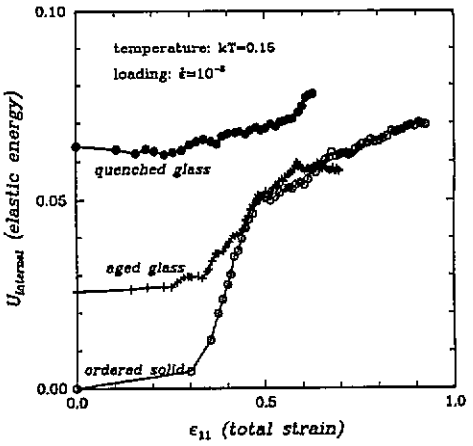

Figure 13. Energy of internal misfit stresses as a function of total strain calculated for the same deformation simulations as figure 12.

found to be of the order of unity (in the reduced units), which means that, among 10 000 elements in the simulation volume, there are quite a few that experience high internal stresses, and are, therefore, first to respond plastically to the imposed deformation. In this situation it is not necessary to create a flow structure, since the initial structure is disordered enough and ready to flow at the applied strain rate of 10^{-3}.

The situation for the aged glass lies in between the two cases discussed above. Unlike the ordered solid, the aged glass configuration has some distribution of internal stresses, which is, however, not wide enough to maintain plastic flow at the required rate from the very beginning. Therefore, a higher level of stress is still necessary in this case to produce the appropriate flow structure, although the yield stress is considerably lower now than it was in the case of the initially ordered structure.

The discussed differences can be further clarified in terms of the internal misfit energy and its changes with plastic flow. This parameter is calculated based on the distribution of internal misfit stresses, and characterizes a degree of non-homogeneity of the plastic strain field in the simulation volume. The misfit energy and its evolution for all three initial structures considered here is shown in figure 13. While for the ordered solid the energy is initially zero, it experiences a stepwise change in a narrow interval of strain around the yield point ($\epsilon \simeq 0.4$). The aged glass has a non-zero residual energy, which is, however, lower than required for steady-state flow, and grows with increasing strain in order to reach an equilibrium flow level. This flow level practically coincides with the value obtained for the ordered solid. Unlike the ordered solid and the aged glass, the energy of the quenched glass is initially so high that it even tends to decrease slightly at small strains, which resembles a certain amount of aging produced in the early stages of flow. This effect is rather insignificant, however, as is the subsequent increase in the energy. So, in this case no stepwise change in the energy is observed, which explains the absence of strain softening in figure 12.

Corresponding structural changes are illustrated in figure 14 where the development of the flow structure is shown for the case of the aged glasses, as an example. An initial structure contains substantial residual disorder, as shown in figure 14(*a*), even though the glass was previously aged (for a more complete discussion of structural features of the

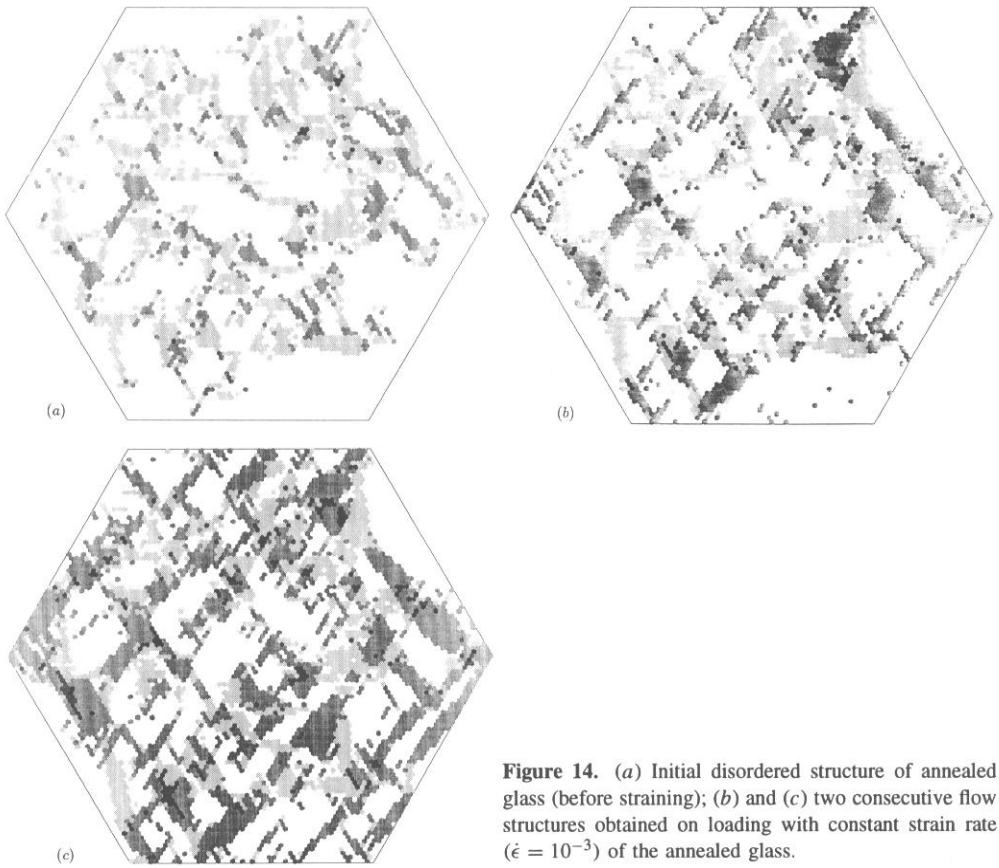

Figure 14. (*a*) Initial disordered structure of annealed glass (before straining); (*b*) and (*c*) two consecutive flow structures obtained on loading with constant strain rate ($\dot{\epsilon} = 10^{-3}$) of the annealed glass.

model solid see II, section 3)†. Plastic flow is localized from the very beginning, as is seen in figure 14(*b*), where a configuration corresponding to a state of flow very near the yield point is shown. Shear bands are initiated in the domains with highest disorder, and propagate throughout the volume. These bands are, however, not so perfect in this case, in comparison to those in figure 6, so that many remnants of the initial disordered structure may be seen even in the stages of well developed plastic flow, as is clear from figure 14(*c*).

In order to observe structural changes produced in the process of flow separately, which are not obscured by the initial disorder, a structure was generated where only incremental changes in the plastic strain field accumulated in flow are shown, as if the initial structure were perfectly ordered. The resulting plot, given in figure 15, is quite different from the corresponding total configuration (figure 14(*c*)). The incremental flow structure appears to be more homogeneous, that is, less localized than the total configuration, which can be viewed as the superposition of the initial disordered structure (figure 14(*a*)) and the incremental flow structure (figure 15). This effect may be related to the fact that in the initial disordered structure there are many local arrangements of LITs with very high local

† Unfortunately, the complexity of the structures considered here is poorly accentuated in the black and white representation used here, where only the amplitudes of local plastic strain are shown. However, additional degrees of freedom (color, hatch pattern, etc) were introduced in order to find a better graphical representation of the (tensorial) plastic strain field. In the future it is intended to develop a more complete representation still suitable for journal publications.

misfit stresses, which later develop in multiple, but irregularly shaped shear bands.

It should be noted here that on further deformation, while the distinctions between the flow structure of the initially ordered solid and the total (superimposed) flow structure of the aged glass gradually vanish, the incremental configuration still displays certain features of the initial disorder in the form of a ghost image.

4.2. Strain-rate and pressure effects

Two stress–strain curves obtained in simulations of deformation of the quenched glass configuration with two different strain rates at $kT = 0.15$ are shown in figure 16. Actually, the lower curve is the same as that shown in figure 12, but the upper curve was obtained at a higher strain rate of $\dot{\epsilon} = 10^{-2}$. Such an order of magnitude increase in strain rate requires a considerably higher level of steady-state stress, as is shown in figure 16. However, no strain softening developed in this case, which suggests that the initial disorder was sufficient for plastic flow to develop smoothly, with no initiation required. It is expected, however, that at still higher strain rates strain softening may be produced even for the highly disordered structure of quenched glass.

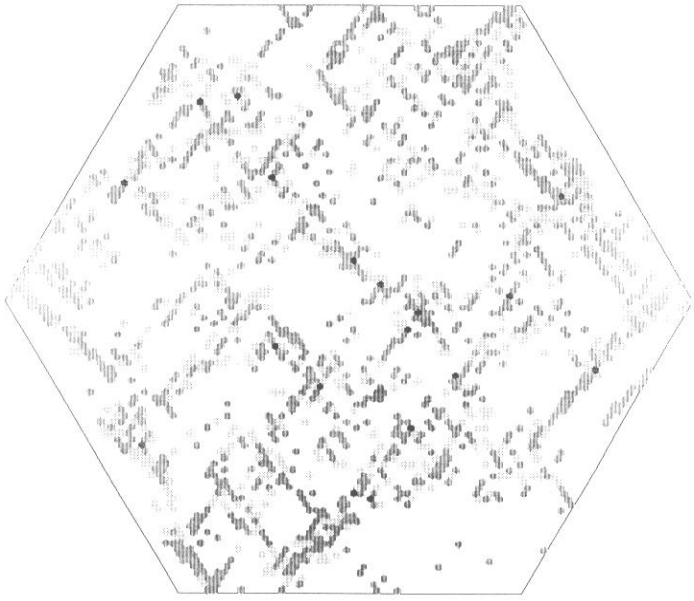

Figure 15. The incremental flow structure of the annealed glass corresponding to the same state of flow as figure 14(*c*).

As was discussed in subsection 3.3, an increase in strain rate produces, in the present model, exactly the same effect on the stress–strain curves as does additional hydrostatic pressure. This means that the upper curve displayed in figure 16, that was obtained at the higher strain rate $\dot{\epsilon} = 10^{-2}$, can be interpreted as obtained at the lower rate $\dot{\epsilon} = 10^{-3}$, but under a higher hydrostatic pressure of

$$\Delta p = 0.5 \times \log_e(10) \simeq 1.15. \tag{4}$$

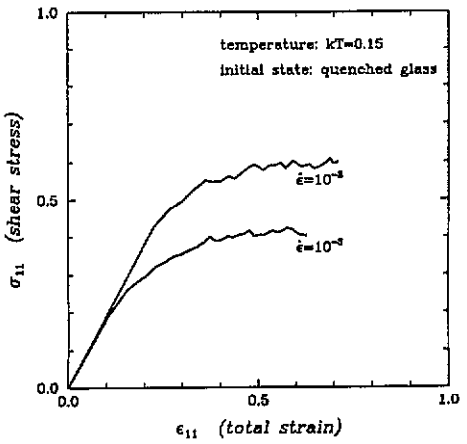

Figure 16. Stress–strain curves obtained on deforming with different strain rates of the quenched glass.

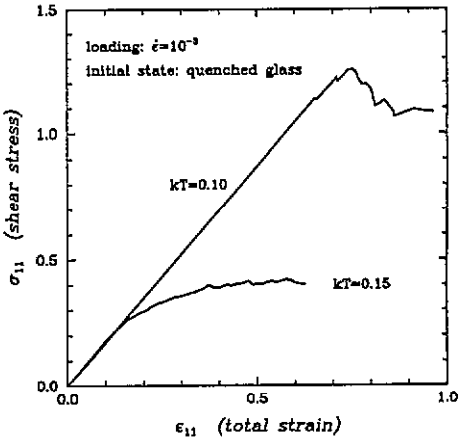

Figure 17. Stress–strain curves obtained on loading of the quenched glass with the same strain rate ($\dot{\epsilon} = 10^{-3}$) but at different temperatures.

4.3. Temperature effect

The results obtained in the simulations of deformation of the quenched glass with the same strain rate $\dot{\epsilon} = 10^{-3}$ but at two different temperatures are presented in figure 17. The upper curve was obtained at the lower temperature $kT = 0.1$, while the lower curve was obtained at the higher temperature $kT = 0.15$, and is the same as the one shown in figure 12 (the lower curve) and figure 16 (the lower curve). In the lower-temperature case a much higher yield stress and subsequent strain softening were produced. The shape of the low-temperature curve implies that, although the initial quenched configuration contains a high density of pre-nucleated shear bands, they are short and become super-critical only at a rather high level of applied stress. Of course, speculations of the same kind should also apply for the higher-temperature case, where the temperature is still much lower than the transition point. It was not expected, therefore, that the difference in flow kinetics for the two simulations discussed would be so great.

Although the reasons for such behavior remain somewhat unclear, a more detailed analysis of structural alterations on the early stages of deformation suggested that the relatively low level of yield stress observed in the higher-temperature simulation is probably due to particular reorganization under external stress of initial disordered domains into pre-nuclei of shear bands that become super-critical at some lower external stress. Such reorganization of the excess disorder into super-critical shear bands is more likely to occur at higher temperatures, where structural relaxations are not yet fully arrested.

Another unexpected result in that the observed amount of strain softening in the lower-temperature case is very small, which is due to the influence of the rigid boundary conditions, which tend to produce artefacts, such as physically unsound stress concentrations and increasingly high misfit energies, at strains higher than 0.8 (see also the discussion in the previous section).

4.4. Cyclic loading of the aged glass

As was mentioned above, development of plastic flow structures depends on the initial disordered structural states of the system. The question, however, is: 'how strong is

such an influence?', or, stated alternatively, 'how long are the initial disordered structures remembered in the process of deformation?'

An attempt to answer this question is made here based on the results of simulations performed on the aged glass under cyclic loading conditions. First, a constant strain rate was applied until a total deformation of $\epsilon = 1.5$ † was reached. Then, the direction of loading was reversed and the system was unloaded at the same strain rate ($\dot{\epsilon} = 10^{-3}$). The reverse loading was continued further beyond the neutral point ($\epsilon = 0$) until a total deformation of $\epsilon = -1.5$ was reached. Then, the direction of loading was reversed again, and a total deformation of $\epsilon = 1.5$ was produced to complete the cycle.

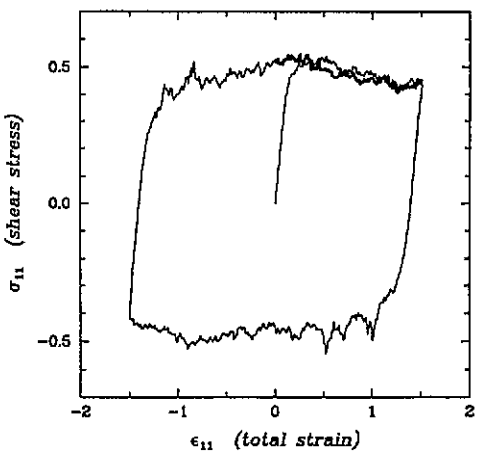

Figure 18. Stress–strain curves obtained in simulations of cyclic loading with constant strain rate ($\dot{\epsilon} = \pm 10^{-3}$) at constant temperature ($kT = 0.15$).

The corresponding stress–strain curve is shown in figure 18, and its general appearance is very close to what was observed in the relevant experiments on cyclic loading [17]. It is interesting to note, though, that on the second passing of the neutral point the model solid still showed some strain softening, which was of about the same magnitude as that produced on the first loading run. After a few more loading cycles were performed, the character of the stress–strain curve remained generally the same.

Analysis of the corresponding structural alterations revealed that plastic flow is initiated in highly disordered regions of the initial structure, and that the developing flow structure is irregular, as was discussed earlier. In the unloading regime most of the shear bands produced earlier disappear, although a few appear to be relatively stable. On further loading in the reverse direction shear bands with plastic strain of the opposite sign are produced. They are initiated in the regions of high disorder, but not at exactly the same sites as on the forward loading. After the direction of loading is reversed again, most of the 'negative' shear bands disappear, and after the second passing of the neutral point the evolution of flow structure is largely repeated, although not in detail.

† It is due to the particular choice of the basic units that the values of yield stresses and yield strains appearing in the discussion are so much higher than those usually observed in experiments. In order to recover all the results in more acceptable magnitudes both stresses and strains should be multiplied by the factor e_s^*, which is expected to be in the range from 0.01 to 0.2 [18] (see also I for details).

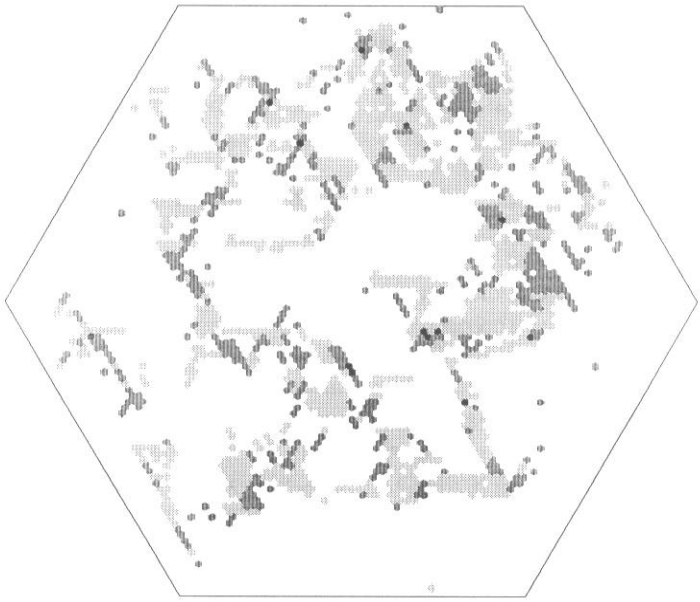

Figure 19. Flow structure obtained on the second passing of the neutral point ($\epsilon = 0$) in the simulations of cyclic loading.

However, more important for the present discussion is the fact that the structure of the solid in the neutral point, after the full loading cycle is completed, is very similar to the initial disordered structure before loading (figure 19). It is our impression that the structure in the neutral point remains almost the same, except for some relatively minor changes, even after a few more runs of the cyclic loading are applied. In other words, the major skeleton of the disordered structure is remarkably stable under conditions of cyclic loading, which contrasts with the results of similar situations performed on the initially ordered structure. This emphasizes an exceptionally strong influence of the initial disordered structure of glass on the development of flow structure on loading.

Further work is needed in order to determine how repeated loadings affect the structure, and, specifically, to find out how many cycles of loading are sufficient for the glass to eventually lose the memory about its initial state, and to what extent the cyclically responding flow units are reversible.

5. Conclusions

The model that was proposed and developed in I and II was used here for simulations of plastic flow under constant strain rate conditions. As was discussed in the preceding papers the model was capable of giving qualitatively correct descriptions of different types of inelastic response in solids, ranging from quasi-Newtonian flow typical of liquids to highly localized flow resembling dislocation glide in crystals at low deformation temperatures (I), and from melting-like equilibrium transitions to relaxation behavior, mimicking kinetic features of the glass transition (II). In general, the results of the simulations discussed in the present communication confirm the ability of the model to account in principle for kinetic and structural features of plastic flow in more or less disordered solids. Some of the effects reproduced correctly include strain softening, strain rate, pressure, and temperature dependences of the plastic response at constant state rate and cyclic loading conditions.

We have also compared kinetic and structural aspects of plastic flow in model solids at similar loading conditions but with different initial structures ranging from defect-free configurations—'perfectly ordered solids'—to fast undercooled, highly disordered configurations—'glasses'. The character of plastic flow appeared to be strongly affected by the degree of initial disorder: while initially ordered solids showed a prominent strain softening behavior, the disordered 'glasses' did not.

As was proposed in I, plastic behavior was analyzed here in terms of the distributions of internal misfit stresses. However, two more parameters pertinent to the processes discussed above were considered here as well: elastic energy of the internal misfit stresses and characteristic length of the shear band pre-nuclei.

The degree of success of the proposed approach suggests that, in spite of the fact that the model used here is very simple, its general applicability for descriptions of the processes of interest has been demonstrated. This emphasizes again an important role of long-range elastic interactions between plastically transformed regions in inelastic processes in solids.

In fact, the only critical assumption in the present model was that various inelastic processes in solids have a common microscopic origin, i.e., local inelastic transformations involving relatively small pieces of solid structure. The present development shows that this assumption is not only conceptually appealing, but also provides the basis for a very effective numerical approach.

Acknowledgments

This research was supported by a DARPA/URI program through the ONR under contract N00014-86-K-0768. Salary support for VVB was provided from a special fellowship from the William and Mary Greve Foundation and from an Allied Signal Corporation Fellowship for which we are grateful to Drs John Kiser and Lance Davis, respectively.

References

[1] Bulatov V V and Argon A S 1994 *Modelling Simul. Mater. Sci. Eng.* **2** 167
[2] Bulatov V V and Argon A S 1994 *Modelling Simul. Mater. Sci. Eng.* **2** 185
[3] Argon A S 1993 *Material Science and Technology* vol 6, ed R W Cahn, P Haasen and E J Kramer (Weinheim: VCH) p 461
[4] Perez J 1982 *Plastic Deformation of Amorphous and Semi-crystalline Materials* ed B Escaig and C G'Sell (Les Ulis: Les Editions de Physique) p 265
[5] Mura T 1987 *Micromechanics of Defects in Solids* (Dordrecht: Martinus Nijhof) p 2
[6] Halsey G, White H J and Eyring H 1945 *Text. Res. J.* **15** 295
[7] Reichl L E 1987 *A Modern Course in Statistical Physics* (Austin, TX: University of Texas Press) p 157
[8] Binder K 1986 *Monte Carlo Methods in Statistical Physics* ed K Binder (Berlin: Springer) p 30
[9] Argon A S 1973 *Phil. Mag.* **28** 389
[10] Teodosiu C 1982 *Elastic Models of Crystal Defects* (Berlin: Springer) p 260
[11] Nemat-Nasser S, Iwakuma T and Hejazi M 1982 *Mech. Mater.* **1** 239
[12] Johnston W G 1962 *J. Appl. Phys.* **33** 2716
[13] Kocks U F, Argon A S and Ashby M F 1975 *Thermodynamics and Kinetics of Slip (Progress in Material Science Series)* (Oxford: Pergamon) p 23
[14] Ashby M F and Jones D R H 1991 *Engineering Materials I* (Oxford: Pergamon) p 125
[15] Hart E W, Li C Y, Yamada H and Wire G L 1975 *Constitutive Equations in Plasticity* ed A S Argon (Cambridge, MS: MIT Press) p 149
[16] Rabinowitz S, Ward I M and Perry J S C 1970 *J. Mater. Sci.* **5** 29
[17] Grosskreutz J C and Mughrabi M 1975 *Constitutive Equations in Plasticity* ed A S Argon (Cambridge, MA: MIT Press) p 251
[18] Mott P, Argon A S and Suter U W 1993 *Phil. Mag.* **67** 931